

AN EXPERIMENTAL STUDY OF THE INFLUENCE OF THE
TURBULENT BOUNDARY LAYER ON
PANEL FLUTTER

By Lado Muhlstein, Jr., Peter A. Gaspers, Jr.,
and Dennis W. Riddle

Ames Research Center
Moffett Field, Calif.

NATIONAL AERONAUTICS AND SPACE ADMINISTRATION

For sale by the Clearinghouse for Federal Scientific and Technical Information
Springfield, Virginia 22151 - CFSTI price \$3.00

AN EXPERIMENTAL STUDY OF THE INFLUENCE OF THE
TURBULENT BOUNDARY LAYER ON
PANEL FLUTTER

By Lado Muhlstein, Jr., Peter A. Gaspers, Jr.,
and Dennis W. Riddle

Ames Research Center

SUMMARY

Flutter dynamic pressure and flutter frequency were obtained for a rectangular unstressed isotropic panel with all edges clamped for the following sets of parameters: (a) Panel length-to-width ratio of 0.5, Mach number range of 1.05 to 1.40, and ratio of boundary-layer thickness to panel length of 0.032 to 0.111; (b) panel length-to-width ratio of 2.0, Mach number of 1.20, and ratio of boundary-layer thickness to panel length of 0.016 to 0.056. For the configurations tested, it is shown that the turbulent boundary layer has a large stabilizing influence on the flutter of flat panels. The effect on flutter dynamic pressure is maximum near $M = 1.20$ and decreases rapidly with increasing Mach number. The effect on flutter frequency is minimum near $M = 1.20$ and increases with increasing Mach number.

INTRODUCTION

There continues to be substantial disagreement between theoretical and experimental panel flutter results in the low supersonic speed range (refs. 1 and 2). It has been suggested (ref. 2), and some experiments have indicated (ref. 3), that part of the disagreement may be due to the presence of the turbulent boundary layer. The influence of the boundary layer on panel flutter has particular significance for large launch vehicles and large supersonic aircraft because the boundary-layer thickness on substantial portions of such vehicles may not be small relative to panel dimensions. Prior to the present investigation, there has been no systematic experimental evaluation of the effect of the boundary layer on panel flutter.

In recent years a number of experimental studies (refs. 1-5) of the flutter of flat isotropic panels in low supersonic flows have been published. Experimental information on boundary-layer effects is contained in references 3 and 5. Reference 3 shows that a small variation in boundary-layer thickness produces a significant change in flutter dynamic pressure; whereas reference 5 shows that a large change in boundary-layer thickness causes essentially no change in the flutter phenomena. However, in reference 5, a number of experimental difficulties such as large temperature gradients in the panel and nonuniform static pressure distributions were noted which raise questions about the reliability of the results.

All the above data show considerable scatter and substantial disagreement with theory. These disparities have been attributed to various sources in addition to the viscous boundary layer, among which are static pressure differential, thermal stresses, built-in stresses, cavity effects, inaccurate or unknown panel edge conditions, nonuniform or unknown flow conditions, unknown structural damping, wind-tunnel-wall effects and imprecise methods of defining the flutter boundary.

A number of theoretical analyses (refs. 6-9) of the effects of the boundary layer on panel flutter have been published. All have concluded that the boundary layer can significantly affect panel flutter, particularly in the low supersonic speed range; but unfortunately all of them suffer from various inadequacies, such as being restricted to two-dimensional panels, being restricted to infinite chord panels, being based on two-dimensional aerodynamics, or oversimplification of the boundary-layer model, and thus do not allow reasonable quantitative comparisons with experiment.

The purpose of the present study was to eliminate as many as possible of the usual sources of experimental inaccuracy, and in particular, to obtain quantitative information concerning the influence of the turbulent boundary layer on panel flutter in the low supersonic speed range.

The flutter boundary was determined for an unstressed rectangular panel with clamped edge conditions for ratios of length to width of 0.5 over the Mach number range of 1.05 to 1.40 and 2.0 at $M = 1.20$. The geometric boundary-layer thickness was varied from approximately 0.25 to 1.0 inch.

SYMBOLS

a	panel dimension in streamwise direction, in.
b	panel dimension in cross-stream direction, in.
C_p	pressure coefficient, $\frac{p - p_\infty}{q_\infty}$
$C_{p_{rms}}$	<u>root-mean-square value of surface pressure fluctuations</u> q_∞
c	speed of sound, ft/sec
E	modulus of elasticity, lb/in. ²
f	frequency, Hz
H	wall displacement, in.
h	panel thickness, in.

K	supersonic reduced frequency, $\frac{kM}{\beta^2}$
k	stiffness parameter, $\sqrt{\frac{\tau^2 E}{c_\infty^2 \rho_s (1 - \nu^2)}}$
k	reduced frequency, $\frac{2\pi fa}{U_\infty}$
M	free-stream Mach number
p	static pressure, lb/ft ²
p _t	total pressure, lb/ft ²
Δp	cavity differential pressure, p _c - p _∞ , lb/ft ²
q	dynamic pressure, $\frac{\rho_\infty U_\infty^2}{2}$, lb/ft ²
T	static temperature, °R
T _t	total temperature, °R
ΔT	panel differential temperature, (T _{panel} - T _{frame}), °F
U	velocity, ft/sec
w	peak panel displacement at transducer location, in.
y	distance from wall to position in boundary layer, in.
α	coefficient of thermal expansion, in./in./°F
β	$\sqrt{M^2 - 1}$
δ	boundary-layer geometric thickness, distance from wall to point where $\frac{U}{U_\infty} = 0.98$, in.
δ _{M=1.0}	distance from wall to point in boundary layer where M = 1.0, in.
δ*	boundary-layer displacement thickness, $\int_0^\delta \left(1 - \frac{\rho U}{\rho_\infty U_\infty}\right) dy$, in.
θ	boundary-layer momentum thickness, $\int_0^\delta \frac{\rho U}{\rho_\infty U_\infty} \left(1 - \frac{U}{U_\infty}\right) dy$, in.

μ	mass ratio parameter, $\frac{\rho_{\infty} a}{\rho_s h}$
μ_c	cavity mass ratio parameter, $\frac{\rho_c a}{\rho_s h}$
ν	Poisson's ratio
ρ	density, slugs/ft ³
τ	panel thickness-to-length ratio, $\frac{h}{a}$

Subscripts

c	cavity
F	flutter
s	structure (panel)
∞	free stream

APPARATUS

Panel Configuration

Dimensional and mounting details of the panel and frame are shown in figure 1. The 9.00-inch by 18.00-inch by 0.0401-inch-thick panel was machined from a single piece of AZ31B-H24 magnesium alloy, 11.00 inch by 20.00 inch by 0.100 inch. The active part of the panel was milled to final dimensions in a series of machining passes and was stress relieved after each pass to eliminate internal stresses and to maintain flatness. This construction produced a panel integral with a surrounding frame which was more than 15 times as stiff as the panel. This frame was attached to a secondary magnesium frame, 1.0 inch wide by 0.50 inch thick, with counterbored button head screws which produced a clamping force without introducing midplane stresses. The resulting combined frame is more than 3300 times as stiff as the panel. This construction was used to closely simulate clamped edge conditions while maintaining a stress free panel.

The panel frame was attached to the test fixture by one high stiffness and two low stiffness flexures as shown in figure 1. This three point mounting was designed to minimize the introduction of external stresses into the panel frame.

Wind Tunnel

The experiments were conducted in the Ames 2- by 2-foot transonic wind tunnel, which is of the continuous flow type with porous test section walls surrounded by a plenum chamber (see ref. 10). Mach number is continuously variable over the range from 0.60 to 1.40, and dynamic pressure is continuously variable over the range from 200 to 1500 psf.

Variable Boundary-Layer Test Fixture

The fixture for varying the boundary-layer thickness consisted of a splitter plate with a sharp leading edge installed in one side wall of the wind tunnel. This splitter plate could be positioned by remote control to be flush with the wall or to project into the airstream up to 1.0 inch. Dimensions of the test fixture are shown in figure 2, and front and rear view photographs are shown in figure 3. When the splitter plate is flush with the tunnel wall, the boundary-layer thickness in the test region is a maximum. When the splitter plate is moved into the airstream, a portion of the tunnel wall boundary layer is directed into the plenum chamber surrounding the test section and a thinner boundary layer is established on the splitter plate. The boundary-layer thickness in the panel test region is variable by this means between the approximate limits of 0.25 and 1.00 inch. Four retractable boundary-layer total-pressure probes were employed to measure boundary-layer thickness at the points shown in figure 2. The variable boundary-layer test fixture containing the test panel is shown installed in the side wall of the 2- by 2-foot transonic wind tunnel in figure 4.

Other Equipment

The panel was backed by a sealed rectangular cavity with the same dimensions as the panel and with an effective depth of 7.5 inch (where effective depth is defined as the actual cavity volume minus volume occupied by instrumentation all divided by panel area). The panel frame was sealed to the cavity with adhesive plastic tape to minimize the possibility of introducing stress into the panel frame.

The differential pressure between the cavity and the free stream was controlled manually to ± 0.25 psf by a system similar to that described in reference 1.

The amplitude of flutter could be controlled by the pressure differential between the cavity and free stream. As an additional safety feature, mechanical "flutter stoppers" were installed in the panel cavity. The "flutter stoppers" consisted of double-acting pneumatic cylinders topped with sponge rubber pads, which, when the cylinders were activated, pressed the pads against the panel surface and stopped the flutter motion mechanically.

PANEL NATURAL FREQUENCIES

To determine the degree to which the panel conformed to the theoretical model of a homogeneous, unstressed panel with clamped edge conditions, the natural frequencies and associated node lines were determined experimentally. Because the natural frequencies are influenced by many quantities, among which are the stiffness and density of the panel material, the density of the air surrounding the panel, the depth of the cavity behind the panel, and stresses such as those produced by a temperature difference between the panel and frame, the effect of each of these variables was determined.

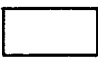


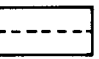

Panel Stiffness

Panel stiffness was determined by measuring the deflection in the center of the panel with a noncontacting capacitive type displacement transducer while applying a uniformly distributed load with differential air pressure and applying equations presented in reference 11. The modulus of elasticity of 5.6×10^6 psi was computed on the basis of average measured panel thickness of 0.0401 inch and an assumed Poisson's ratio of 0.35. Panel thickness was determined with an ultrasonic thickness measuring instrument and material density was determined by weighing a sample in air and in water.

Air Density Effects

The effect of air density on natural frequencies, with the panel backed by a 7.5-inch-deep cavity essentially identical to the one used during the wind-tunnel test, is shown in figure 5 by the change of panel natural frequencies with air pressure. These natural frequencies can be extrapolated to zero pressure where there will be no air density or cavity effects. In the following table these frequencies are compared with theoretical in vacuo values determined by a 196-mode (14 modes in each direction) Galerkin solution utilizing clamped beam modes (ref. 12). The measured node lines associated with each natural frequency are also shown. This comparison indicates that the panel conforms within 1 percent to the theoretical model for the first two natural frequencies. It will be noted that the mode shapes for the fourth and fifth measured natural frequencies are in reverse order from theory. This switch in mode shape sequence can easily be accounted for by an approximately 5 percent difference in stiffness between the panel axes. This difference in stiffness could result from the use of rolled material for fabricating the panel as well as from the panel support system which is more rigid along the short panel axes. Because the primary interest in this investigation is in the first two panel natural frequencies, it can be said that the panel conforms very well to the above theoretical model.

Panel Natural Frequencies and Locations of Node Lines

Location of node lines					
Measured natural frequencies, Hz	110	143	212	287	298
Computed natural frequencies, Hz	109.7	142.0	199.8	285.5	282.6
Deviation of measured natural frequencies from computed values, percent	0.27	0.70	6.11	0.53	5.45

Cavity Depth Effects

The effect of cavity depth on the natural frequencies of the unstressed panel at atmospheric pressure is shown in figure 6. These data were obtained with an unvented variable depth cavity with all walls more than 1000 times as stiff as the panel. These results indicate that a 7.5-inch-deep cavity at atmospheric pressure will increase the first natural frequency approximately 9.4 percent above the in vacuo natural frequency, but will change the higher natural frequencies less than 2 percent. Since all flutter data presented in this report were taken at static pressures between 0.25 and 0.65 atmospheres, the influence of the cavity on these data will be less than indicated above. Figure 6 also indicates that for a very shallow cavity, the natural frequency for the first mode is higher than for the second mode, which agrees with the information presented in reference 13. The natural frequencies presented in figures 5 and 6 were determined by the forced vibration technique of reference 14.

Thermal Effects

The theoretical effect on panel natural frequencies of a uniform temperature differential between the panel and frame is shown in figure 7 for compressive resultant stress. The temperature at which the first natural frequency goes to zero corresponds to buckling of the panel (ref. 15), in this case 3.3° F. This figure indicates that small temperature differentials can have a large effect on panel natural frequencies and, consequently, a large effect on the flutter boundary.

In actual practice it is not possible to get a uniform temperature differential because of thermal conduction between the panel and frame; thus, an experiment was conducted to determine the actual effect of temperature differentials on natural frequencies. The panel was radiantly heated very rapidly and its natural frequencies were determined for various temperature differentials. In an attempt to conform as nearly as possible to theory, the

frame was insulated from the heat source, and heat was concentrated near the panel boundaries to compensate for conduction into the frame. Typical temperature distributions measured on the unheated side of the panel for various times from start of heating are shown in figure 8. The panel natural frequencies were determined by spectral analysis of the transient displacement signal resulting from periodically exciting the panel with a mechanical impulse during the heating cycle. The natural frequencies as a function of temperature differential between the frame and the center of the panel are shown in figure 9. Buckling was observed at a differential temperature of approximately 12° F which coincides with the differential temperature for minimum resonant frequencies. The difference between theory and experiment in buckling temperature is probably due to the inability to obtain a step change in temperature at the boundary because of thermal conduction and also to possible panel curvature due to temperature differentials through the panel caused by heating on only one side (ref. 15).

The above experiment indicates that a $\pm 0.5^{\circ}$ F temperature differential will change the first natural frequency less than 2 percent. Thus it is expected that a temperature differential of this magnitude would have a correspondingly small effect on the flutter boundary (ref. 16). Consequently, the panel-frame temperature differential was maintained at less than $\pm 0.5^{\circ}$ F during the wind-tunnel test, with most of the variation being less than $\pm 0.2^{\circ}$ F.

INSTRUMENTATION

Panel displacement was measured with a noncontacting capacitance type transducer which produced an output voltage linearly proportional to the panel displacement. This instrument, which has a range of 0.100 inch, a flat frequency response of dc to 10,000 Hz, and linearity of ± 1.0 percent, was positioned 0.050 inch from the under surface of the panel at the location shown in figure 2.

The steady surface static pressures and the total pressures from the boundary-layer probes were measured with conventional strain gage differential-pressure transducers connected to the orifices by short lengths of tubing and referenced to free-stream static pressure.

The unsteady surface pressures were measured with flush diaphragm pressure transducers with piezoresistive sensing elements. These transducers have a diameter of 0.125 inch, a pressure range of ± 1.0 psi differential, and a flat frequency response of 0 to 12,000 Hz, and were referenced to a local surface static pressure through a length of small diameter tubing to damp frequencies above 10 Hz.

Panel and frame temperatures were measured with iron-constantan thermocouples in the center of the panel and at two points on the frame. The thermocouple in the center of the panel was constructed of wire 0.005 inch in diameter and was the only object contacting the panel.

Steady quantities such as temperatures and pressures were recorded digitally. Unsteady or slowly varying quantities such as fluctuating static pressure, panel response, and pressure differential between the cavity and free stream were recorded by a frequency modulated magnetic tape recorder with a frequency response of dc to 1250 Hz.

TEST PROCEDURE

Flow Conditions in Panel Test Region

An important consideration in panel flutter testing is that the surface pressure distribution in the test region be uniform. A nonuniform static pressure distribution would cause local differential pressures between the cavity behind the panel and the free stream which would stress and distort the panel locally, thereby producing erroneous flutter data. Typical values of the surface static pressure coefficient in the test region for the present tests are shown in figure 10. The maximum variation is ± 0.02 , with most variations being less than ± 0.01 .

An additional consideration in panel flutter testing is that fluctuating surface pressures such as those produced by boundary-layer turbulence, free-stream turbulence, and wind-tunnel compressor drive harmonics not contain any strong sinusoidal components in the frequency range where flutter occurs. Such components could cause the panel to exhibit flutter-like response under low damping conditions prior to actual flutter. Representative values of the root-mean-square fluctuating pressure coefficient at $M = 1.20$ for various boundary-layer thicknesses at stations upstream and downstream of the panel test region are shown in figure 11. A typical power spectrum of the fluctuating surface pressure is shown in figure 12. This power spectrum was obtained with a constant bandwidth (5 Hz measured at the 3 dB points) spectrum analyzer with linear sweep from a data sample of approximately 20-seconds duration. The power spectrum indicates that there are no dominant frequencies in the frequency range of interest of the present investigation.

A typical variation of the geometric boundary-layer thickness with splitter plate position is shown in figure 13. Typical velocity profiles along the wall centerline for various splitter plate displacements are shown in figures 14(a) and 14(b) for stations upstream and downstream, respectively, of the panel test region. A $1/7$ th power profile is shown in both figures for comparison.

The effect of the wind-tunnel wall opposite the panel on the flutter boundary will be negligible from purely geometric considerations because acoustic disturbances originating on the panel are reflected downstream for all Mach number and configuration combinations tested. The effects of the wind-tunnel side walls are expected to be small because of geometric considerations as well as the large attenuating effects of the porous tunnel walls and the turbulent boundary layer on these walls as discussed in reference 17.

Determination of the Flutter Boundary

The criterion for a flutter boundary in a theoretical analysis is very simple; however, the experimental determination of this boundary has proved to be very difficult (ref. 1).

From a theoretical viewpoint the flutter boundary is defined as the locus of neutral stability. For a linear theory the stable side of a flutter boundary corresponds to decaying initial disturbances and the unstable side to unbounded amplification of initial disturbances. For a nonlinear theory, the stable side of a flutter boundary again corresponds to decaying initial disturbances but the unstable side is characterized by a limit cycle oscillation for which the amplitude goes to zero as the boundary is approached from the unstable side.

The experimental determination of the flutter boundary is complicated by several factors among which are the nonlinear behavior of clamped plates for finite deflections producing in-plane tension, the presence of a random unsteady pressure field due to boundary layer and free-stream turbulence, slowly changing free-stream conditions, and variation in pressure differential between the cavity and free stream due to the changing free-stream conditions. The random unsteady pressure field produces forced random motion of the panel with largest amplitudes in the frequency spectrum in the vicinity of the natural frequencies of the panel-airstream system. As the flutter boundary is approached from the stable side, the total damping of the system decreases at frequencies near the flutter frequency (ref. 14); consequently, panel amplitude due to the fluctuating pressures will increase. At or near the flutter boundary, the panel-airstream system acts like a narrow band-pass filter with the random pressure field the input and the panel response the output. At the flutter boundary, the limit cycle motion due to flutter is of zero amplitude and so undetectable. As the unstable region is penetrated, the limit cycle grows in amplitude and eventually dominates the random response. Now the output of a narrow band-pass filter with a random input is hard to distinguish from a sinusoid (ref. 18); thus it is difficult to separate the increased random response due to decreased damping from the true flutter response.

The criteria used in past works to define the flutter boundary experimentally have either not been stated at all or only imprecisely. The problem is discussed thoroughly in reference 1 where results are presented in the form of a scatter band for each flutter point, i.e., an upper and lower bound for each flutter point is stated. While this is perhaps the most satisfactory method used to date for presenting experimental results, it leaves the flutter boundary uncertain within the width of the scatter band, and, of course, there remains arbitrariness in selection of the upper and lower limits.

In the present study, the flutter boundary is determined as follows: At dynamic pressures well below that for flutter, the panel response to pressure disturbances from the turbulent boundary layer increases approximately linearly with dynamic pressure, as indicated in figure 15. In this figure, panel amplitude in the mode which becomes the flutter mode is shown as a function of dynamic pressure. This "subflutter response" is used as a reference level to define the flutter point systematically. The straight lines labeled 2x, 3x,

etc., in figure 15 are multiples of the subflutter response. Their intersections with the amplitude response curve define values of dynamic pressure necessary to produce panel amplitudes which are these multiples of the subflutter response. Figure 16 shows dynamic pressure as a function of the multiples of the subflutter response for the same conditions as shown in figure 15. As the multiple increases, the difference in dynamic pressure between successive multiples decreases; that is, the dynamic pressure appears to be converging to a limit. Furthermore it appears that the 6x multiple results in a dynamic pressure very close to this limiting dynamic pressure and is therefore arbitrarily defined herein as the flutter boundary.

The following test procedure was adhered to throughout the program. Mach number and splitter plate position were held constant while dynamic pressure was increased in small increments beginning at a value well below the flutter boundary. After each increase in dynamic pressure, the panel-frame temperature difference was allowed to stabilize to $\pm 0.5^{\circ}$ F to minimize thermal stress effects. The indicated differential pressure between the cavity and free stream was then varied slowly from -50 psf to +50 psf while the panel response was recorded. It is assumed that the maximum response so measured corresponds to zero average differential pressure across the panel. Next the indicated differential pressure was set to the value at which maximum response occurred. This response was recorded so that amplitude spectrums could be obtained with all test conditions fixed. The above procedure was repeated for each increase in dynamic pressure until the maximum response was a large amplitude, essentially sinusoidal motion indicating that the flutter boundary had been penetrated. Boundary-layer velocity profiles were obtained at dynamic pressures near the flutter boundary. The forward probe was retracted while data were being recorded for the rear probes, and all probes were retracted when boundary layer data were not being recorded.

Panel amplitude response at dynamic pressures below flutter was a random waveform in which most of the energy was concentrated near the natural frequencies of the panel-airstream system. The special data reduction system shown in block diagram form in figure 17 was developed to determine the amplitude response of the panel mode which becomes the flutter mode. This system automatically tracks and filters a dominant response peak as its frequency and amplitude vary with differential pressure. The system outputs voltages proportional to the frequency it is tracking and to the amplitude at that frequency. These quantities are automatically plotted as functions of the differential pressure between the cavity and free stream. A representative plot produced by this system is shown in figure 18. Except for the data in figure 19, all panel response and flutter frequency data presented in this report were obtained from such plots.

As noted previously, panel response was also recorded at the fixed differential pressure between the cavity and free stream at which this response was maximum. An amplitude spectrum for such a fixed differential pressure is shown in figure 19. The spectrum was obtained with a constant bandwidth (5 Hz measured at the 3 dB points) spectrum analyzer with linear sweep from a data sample of approximately 20 seconds duration. This figure

corresponds to the same test conditions as those in figure 18 with which it agrees well in both frequency and amplitude.

RESULTS AND DISCUSSION

Influence of the Turbulent Boundary Layer on Flutter Dynamic Pressure

The dynamic pressures for various multiples of subflutter response for a series of boundary-layer thicknesses at $M = 1.20$ are shown in figure 20 for $a/b = 0.5$ and in figure 21 for $a/b = 2.0$. The value of the geometric boundary-layer thickness used is the thickness in the center of the panel estimated by assuming linear growth between the upstream and downstream probes. The curve for $6\times$ subflutter response is considered the flutter boundary. The flutter dynamic pressure in figures 20 and 21 is approximately a linear function of the geometric boundary-layer thickness.

In figures 20 and 21 the rate of change of flutter dynamic pressure with boundary-layer thickness is much greater for the $a/b = 0.5$ case where the panel length is 9.0 inches than for the $a/b = 2.0$ case where the panel length is 18.0 inches. If the boundary-layer thickness is normalized with respect to the panel length (δ/a), as discussed in reference 7, the rate of change of flutter dynamic pressure is much more nearly the same for the two different panel lengths as shown in figure 22, thus indicating that an important parameter in the study of boundary-layer effects is δ/a . However, it should be noted that a/b is not identical; therefore, the two curves would not be expected to be identical.

The dynamic pressure for various multiples of panel subflutter response as a function of Mach number for $a/b = 0.5$ is shown in figure 23 for the maximum geometric boundary-layer thickness (approximately 1.0 in.) and in figure 24 for the minimum geometric boundary-layer thickness (approximately 0.25 in.). In both cases the boundary-layer thickness varies slightly with Mach number. Both figures show the characteristic minimum (refs. 1, 2, 3) in flutter dynamic pressure in the vicinity of $M = 1.20$ and a rapid increase with increasing Mach number.

The approximate linear relationship of flutter dynamic pressure with boundary-layer thickness indicated in figures 20 and 21 is used to show the change of flutter dynamic pressure with boundary-layer thickness ($dq/d\delta$) for $a/b = 0.5$ as a function of Mach number in figure 25. This figure indicates that the maximum boundary-layer effect occurs near $M = 1.20$ and decreases rapidly with increasing Mach number.

By use of a linear relationship of flutter dynamic pressure with boundary layer thickness at all Mach numbers, these data can be reasonably extrapolated to zero boundary-layer thickness to obtain a flutter boundary for comparison with results predicted by potential flow theory. This linear relationship can also be used to derive the flutter dynamic pressures at various other constant boundary-layer thicknesses (for $a/b = 0.5$) shown in figure 26.

Influence of the Turbulent Boundary Layer on Flutter Frequency

The flutter frequencies for various boundary-layer thicknesses at a Mach number of 1.20 are shown for $a/b = 0.5$ and 2.0 in figure 27. Here a linear relationship with geometric boundary-layer thickness is again noted.

The rate of change of flutter frequency with boundary-layer thickness ($df/d\delta$) at $M = 1.20$ is much greater for $a/b = 0.5$ (panel length of 9.0 in.) than for $a/b = 2.0$ (panel length of 18.0 in.) as indicated in figure 27. Normalizing the boundary-layer thickness with respect to the panel length (δ/a) makes the rate of change of flutter frequency with this quantity approximately the same for both values of a/b as shown in figure 28.

Using a linear relationship of flutter frequency to boundary-layer thickness for all Mach numbers, figure 29 is derived showing flutter frequency as a function of Mach number for various constant geometric boundary-layer thicknesses for $a/b = 0.5$. There is some indication from the figure (for $\delta = 0.95$ inch at least) that the flutter frequency approaches zero as Mach number decreases toward 1.0. This is in qualitative agreement with the theoretical results presented in reference 19.

The rapidly increasing flutter frequency in the vicinity of $M = 1.40$ for thin boundary layers is probably associated with the change in the nature of the flutter from single degree of freedom to two mode coupled type as predicted by theory in this Mach number range. Based on results of reference 19, it is expected that for a thin boundary layer, the flutter frequency versus Mach number curve will again level out near $M = 1.60$, after which it will change slowly. For a thick boundary layer the rapid change in frequency would be expected to occur at a higher Mach number.

The rate of change of flutter frequency with boundary-layer thickness ($df/d\delta$) as a function of Mach number for $a/b = 0.5$ is shown in figure 30. The increasing effect of boundary-layer thickness on flutter frequency in the range $M = 1.20$ to 1.40 is probably associated with the rapid change of flutter frequency with Mach number in this region while the increasing effect of boundary-layer thickness below $M = 1.20$ is associated with the rapid decrease of frequency toward zero as Mach number decreases to $M = 1.0$. It is interesting to note from figures 24 and 30, that the boundary layer has minimum effect on flutter frequency and maximum effect on flutter dynamic pressure at approximately the same Mach number of 1.20. From these results, it is clearly evident that ignoring boundary-layer effects may lead to considerable difference between theory and experiment for flutter frequency and/or flutter dynamic pressure at low to moderate supersonic Mach numbers.

Panel Flutter Parameters

A natural set of dimensionless parameters for the flutter of flat isotropic panels exposed to linearized three-dimensional unsteady potential flow (ref. 20) are the mass ratio parameter, $\mu = \rho_\infty a / \rho_s h$, the stiffness parameter, $k = \sqrt{\tau^2 E / c_\infty^2 \rho_s (1 - \nu^2)}$, the panel length-to-width ratio, a/b , the Mach number M , and the reduced frequency k . Flutter boundaries may be plotted in

the μ - k plane for various reduced frequencies for each Mach number and length-to-width ratio. In figure 31 the mass ratio parameter is plotted as a function of boundary-layer thickness for the various Mach numbers. Since these data fall approximately on a straight line, they can reasonably be extrapolated to zero boundary-layer thickness to obtain a value of μ for comparison with results predicted by potential flow theory. Again the influence of the boundary-layer thickness is clearly evident. The reduced frequency as a function of Mach number for various constant geometric boundary-layer thicknesses is presented in figure 32. Computed values of μ and k and other pertinent quantities, such as boundary-layer thickness and dynamic pressure for flutter, are presented for each flutter point in table I.

CONCLUSIONS

1. The turbulent boundary layer has a large stabilizing influence on the flutter of flat isotropic panels at low supersonic Mach numbers.
2. The effect of the turbulent boundary layer on flutter dynamic pressure is maximum near $M = 1.2$ and decreases rapidly with increasing Mach number for the configurations tested.
3. The effect of the turbulent boundary layer on flutter frequency is a minimum near $M = 1.2$ and increases with increasing Mach number over the range $M = 1.2$ to 1.4 for the configurations tested.

Ames Research Center
National Aeronautics and Space Administration
Moffett Field, Calif., 94035, Dec. 5, 1967
126-14-02-01-00-21

REFERENCES

1. Dowell, E. H.; and Voss, H. M.: Experimental and Theoretical Panel Flutter Studies in the Mach Number Range of 1.0 to 5.0. ASD-TDR-63-449, The Boeing Company, Seattle, Washington, 1963. Also, Theoretical and Experimental Panel Flutter Studies in the Mach Number Range 1.0 to 5.0. AIAA J., vol. 3, no. 12, Dec. 1965, pp. 2292-2304.
2. Lock, M. H.; and Fung, Y. C.: Comparative Experimental and Theoretical Studies of the Flutter of Flat Panels in a Low Supersonic Flow. GALCIT 95 or AFOSR 670, Guggenheim Aero. Lab., Calif. Inst. Tech., Pasadena, Calif., May 1961.
3. Hodson, C. H.; and Stocker, J. E.: Commercial Supersonic Transport Panel Flutter Studies. RTD-TDR-63-4036, North American Aviation, May 1964.
4. Sylvester, Maurice A.; and Baker, John E.: Some Experimental Studies of Panel Flutter at Mach Number 1.3. NACA TN 3914, 1957.
5. Dat, Roland; Faure, Gerard; and Chopin, Suzanne: Etude de L'Instabilite Aeroelastique D'un Panneau Rectangulaire Plan. La Recherche Aerospatiale, No. 112, pp. 27-32, May-June, 1966. Also available as - Study of the Aeroelastic Instability of a Flat Rectangular Panel, NASA-TT-F-10645.
6. Miles, John W.: On Panel Flutter in the Presence of a Boundary Layer. J. Aero. Space Sci., vol. 26, no. 2, Feb. 1959, pp. 81-93.
7. McClure, James D.: On Perturbed Boundary Layer Flows. Rep. 62-2, MIT Fluid Dynamics Res. Lab., June 1962.
8. Fung, Y. C.: Some Recent Contributions to Panel Flutter Research. IAS Paper 63-26, 1963.
9. Zeydel, E. F. E.: Study of the Pressure Distribution on Oscillating Panels in Low Supersonic Flow With Turbulent Boundary Layer. NASA CR-691, 1967.
10. Spiegel, Joseph M.; and Lawrence, Leslie F.: A Description of the Ames 2- by 2-Foot Transonic Wind Tunnel and Preliminary Evaluation of Wall Interference. NACA RM A55I21, 1956.
11. Timoshenko, S.; and Woinowsky-Krieger, S.: Theory of Plates and Shells. Second ed., McGraw-Hill Book Co., Inc., N. Y., 1959.
12. Gaspers, Peter A., Jr.; and Redd, Bass: A Theoretical Analysis of the Flutter of Orthotropic Panels Exposed to a High Supersonic Stream of Arbitrary Direction. NASA TN D-3551, 1966.
13. Dowell, E. H.; and Voss, H. M.: The Effect of a Cavity on Panel Vibration. AIAA J., vol. 1, no. 2, Feb. 1963, pp. 476-477.

14. Muhlstein, Lado, Jr.: A Forced-Vibration Technique for Investigation of Panel Flutter. AIAA Paper 66-769.
15. Lurie, Harold: Lateral Vibrations as Related to Structural Stability. J. Appl. Mech., vol. 19, no. 2, June 1952, pp. 195-204.
16. Schaeffer, Harry G.; and Heard, Walter, L., Jr.: Flutter of a Flat Panel Subjected to a Nonlinear Temperature Distribution. AIAA J., vol. 3, no. 10, Oct. 1965, pp. 1918-1923.
17. Goethert, Bernhard H.: Transonic Wind Tunnel Testing. Wilbur C. Nelson, ed., AGARDograph 49, Pergamon Press, 1961.
18. Lee, Y. W.: Statistical Theory of Communication. John Wiley & Sons, Inc., N. Y., 1960.
19. Dowell, E. H.: Nonlinear Oscillations of a Fluttering Plate. II, AIAA J., vol. 5, no. 10, Oct. 1967, pp. 1856-1862.
20. Zeydel, Edmond F. E.: Large Deflection Panel Flutter. AFOSR Tech. Note 1952, Jan. 1962.

TABLE I.- TABULATED PANEL FLUTTER DATA

MACH NUMBER	WALL DISPLACEMENT H, in.	FREE STREAM TEMPERATURE T _∞ , °R	DYNAMIC PRESSURE FOR MULTIPLES OF SUBFLUTTER RESPONSE, PSF					BOUNDARY LAYER THICKNESS, IN.			FLUTTER FREQUENCY	REDUCED FLUTTER FREQUENCY	SUPERSONIC REDUCED FLUTTER FREQUENCY	DENSITY RATIO	CAVITY DENSITY RATIO	STIFFNESS PARAMETER	
			q _{2x}	q _{3x}	q _{4x}	q _{5x}	q _{6x} = q _{1F}	δ	δ _{δ=1.0}	δ*							θ
a/b = 0.5																	
1.05	0.00	445.7	1018	1040	1046	1049	1050	0.95	0.97	0.199	0.088	40	0.174	1.777	0.1173	0.0988	0.0704
1.10	0.00	438.5	945	1000	1015	1025	1035	1.03	0.74	0.210	0.094	70	0.293	1.534	0.1070	0.0888	0.0725
1.10	1.00	436.0	575	605	608	609	609	0.30	0.21	0.085	0.028	92	0.386	2.021	0.0634	0.0523	0.0712
1.20	0.00	422.4	928	972	998	1012	1018	1.02	0.44	0.217	0.099	110	0.428	1.168	0.0918	0.0734	0.0723
1.20	0.20	413.9	775	832	858	873	882	0.77	0.34	0.184	0.076	117	0.458	1.250	0.0812	0.0644	0.0730
1.20	0.40	413.0	687	733	753	763	767	0.52	0.26	0.121	0.052	118	0.463	1.263	0.0708	0.0561	0.0731
1.20	0.60	412.1	653	685	702	712	715	0.46	0.22	0.105	0.044	119	0.469	1.278	0.0661	0.0524	0.0732
1.20	0.80	410.6	625	655	668	680	688	0.34	0.19	0.106	0.034	122	0.481	1.312	0.0639	0.0504	0.0733
1.20	1.00	414.1	562	595	604	605	605	0.28	0.16	0.086	0.028	122	0.478	1.304	0.0557	0.0443	0.0730
1.30	0.00	406.4	960	1050	1077	1090	1098	0.96	0.26	0.208	0.082	126	0.462	0.869	0.0873	0.0674	0.0737
1.30	1.00	408.8	750	835	870	880	882	0.28	0.10	0.081	0.026	148	0.542	1.021	0.0701	0.0537	0.0735
1.40	0.00	403.7	1175	1243	1276	1287	1290	0.89	0.18	0.196	0.079	144	0.492	0.717	0.0895	0.0674	0.0740
1.40	1.00	402.3	1133	1180	1185	1187	1188	0.27	0.08	0.081	0.024	185	0.635	0.926	0.0826	0.0611	0.0741
a/b = 2.0																	
1.20	0.00	414.2	728	738	745	750	752	1.02	0.45	0.264	0.124	114	0.895	2.441	0.1384	0.1100	0.0365
1.20	0.20	412.8	663	683	686	688	690	0.90	0.33	0.172	0.086	115	0.899	2.452	0.1274	0.1008	0.0366
1.20	0.40	412.6	606	623	635	642	648	0.61	0.26	0.128	0.058	116	0.907	2.473	0.1197	0.0948	0.0366
1.20	0.60	414.1	586	605	616	623	627	0.46	0.19	0.102	0.042	117	0.922	2.515	0.1154	0.0918	0.0365
1.20	1.00	416.8	510	568	586	595	598	0.30	0.16	0.085	0.030	118	0.923	2.518	0.1094	0.0870	0.0364

PANEL CHARACTERISTICS

Panel dimensions 9.000 x 18.000 x 0.0401 in. thick
 Edge conditions Clamped all sides
 Material Magnesium alloy AZ 31B-H24
 E 5.6x10⁶ psi
 ν 0.35
 ρ_s 110.0 lb/ft³
 α 14.2x10⁻⁶ in./in./°F

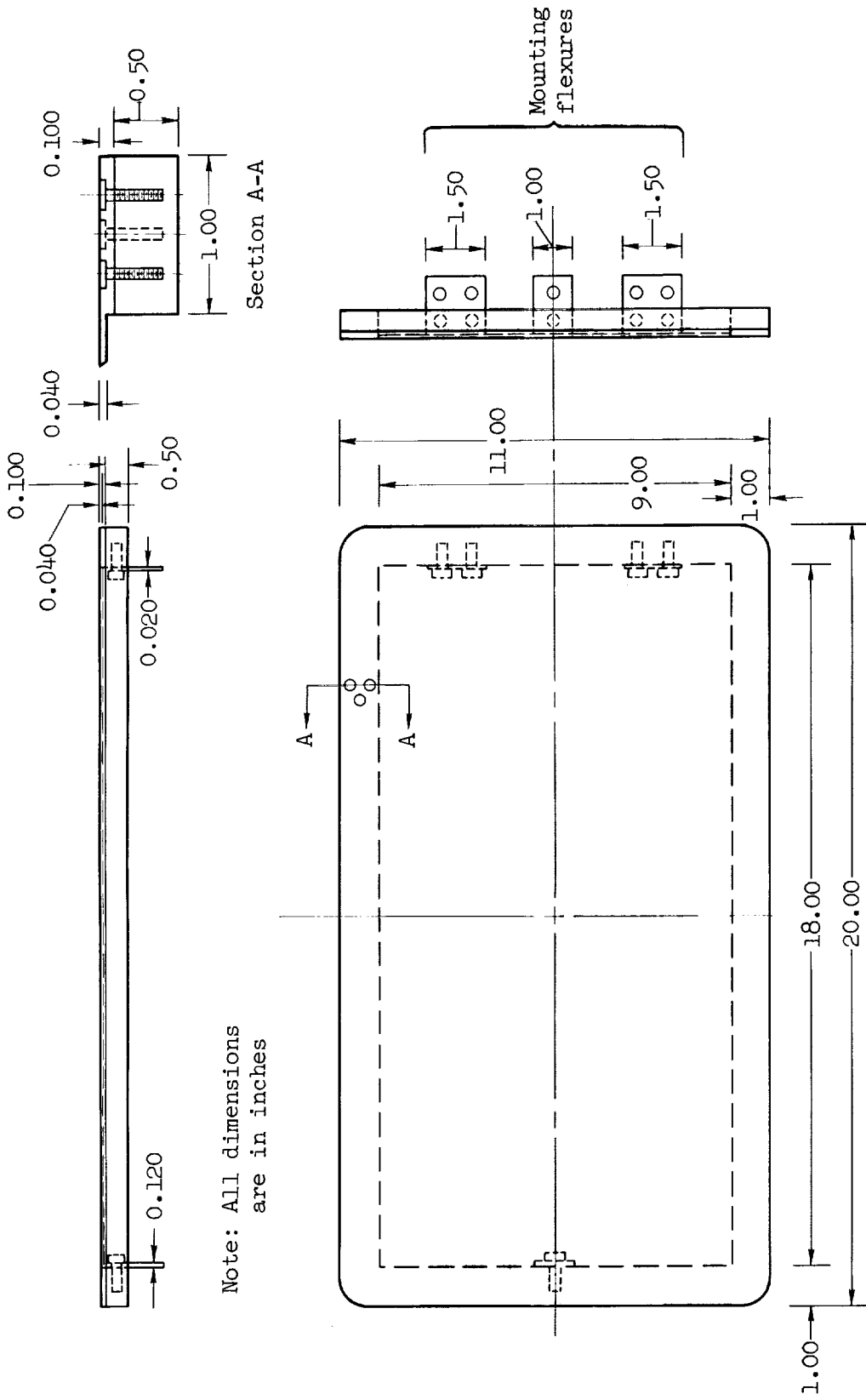


Figure 1.- Panel dimensions and construction details.

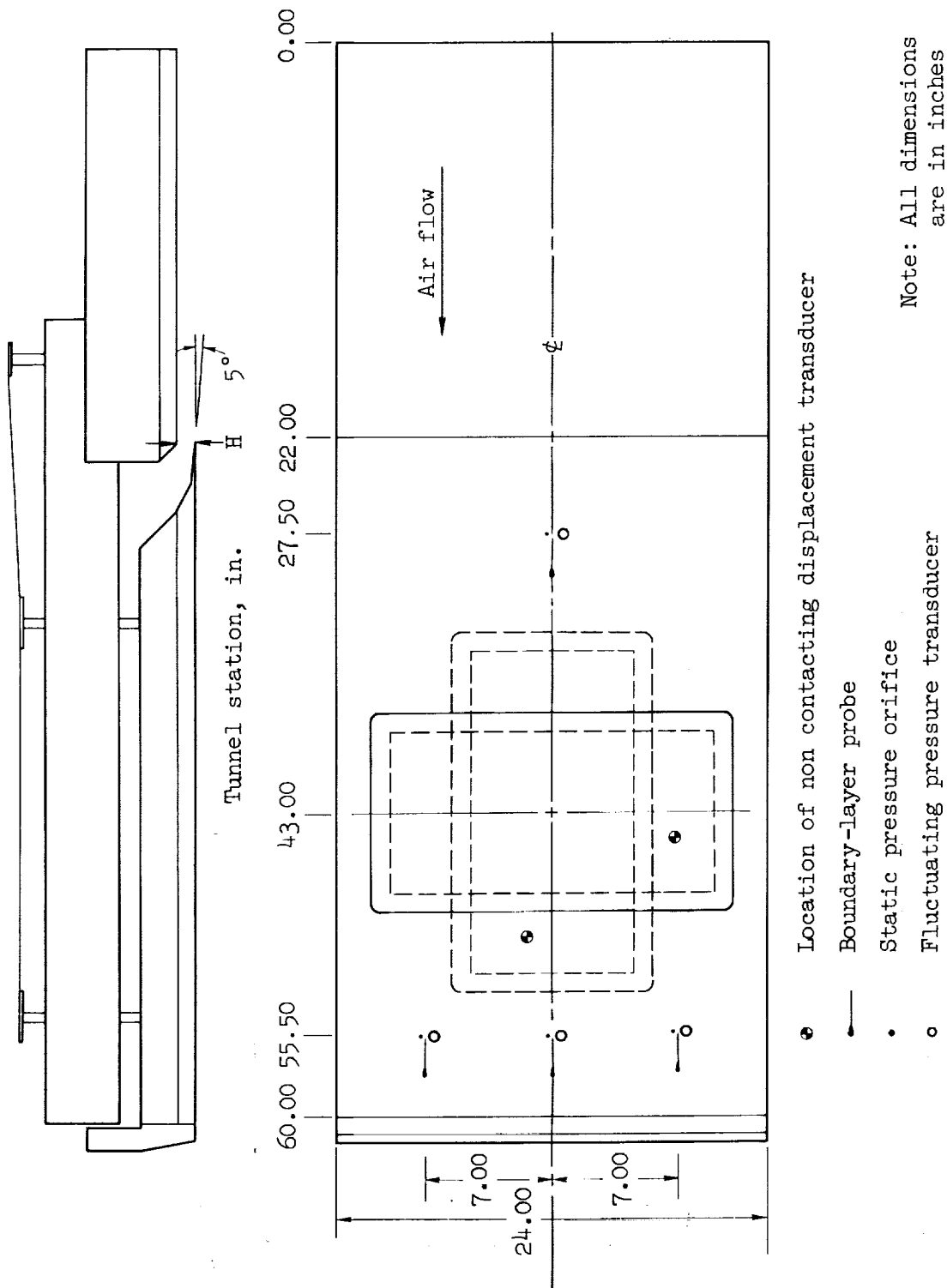
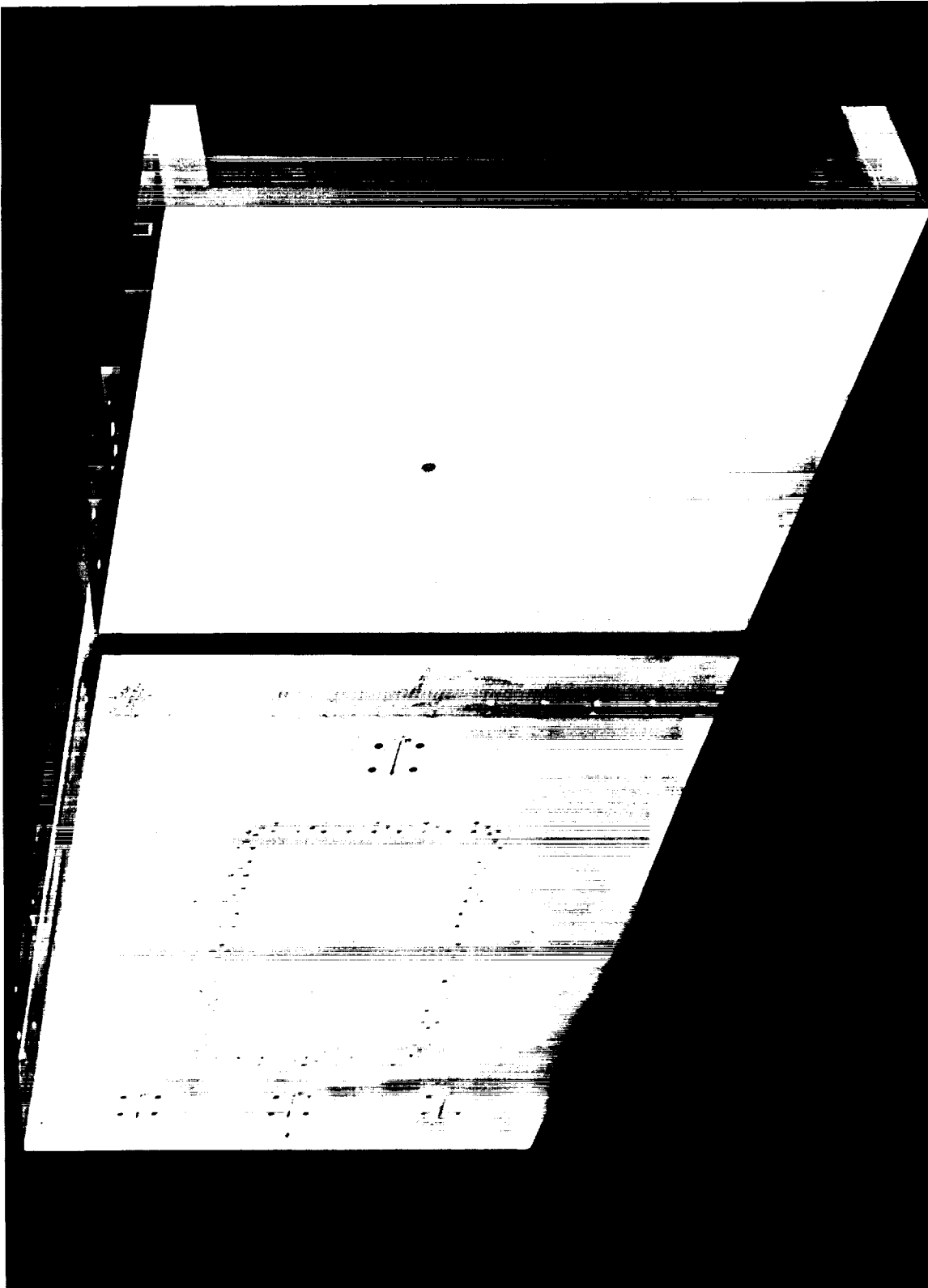
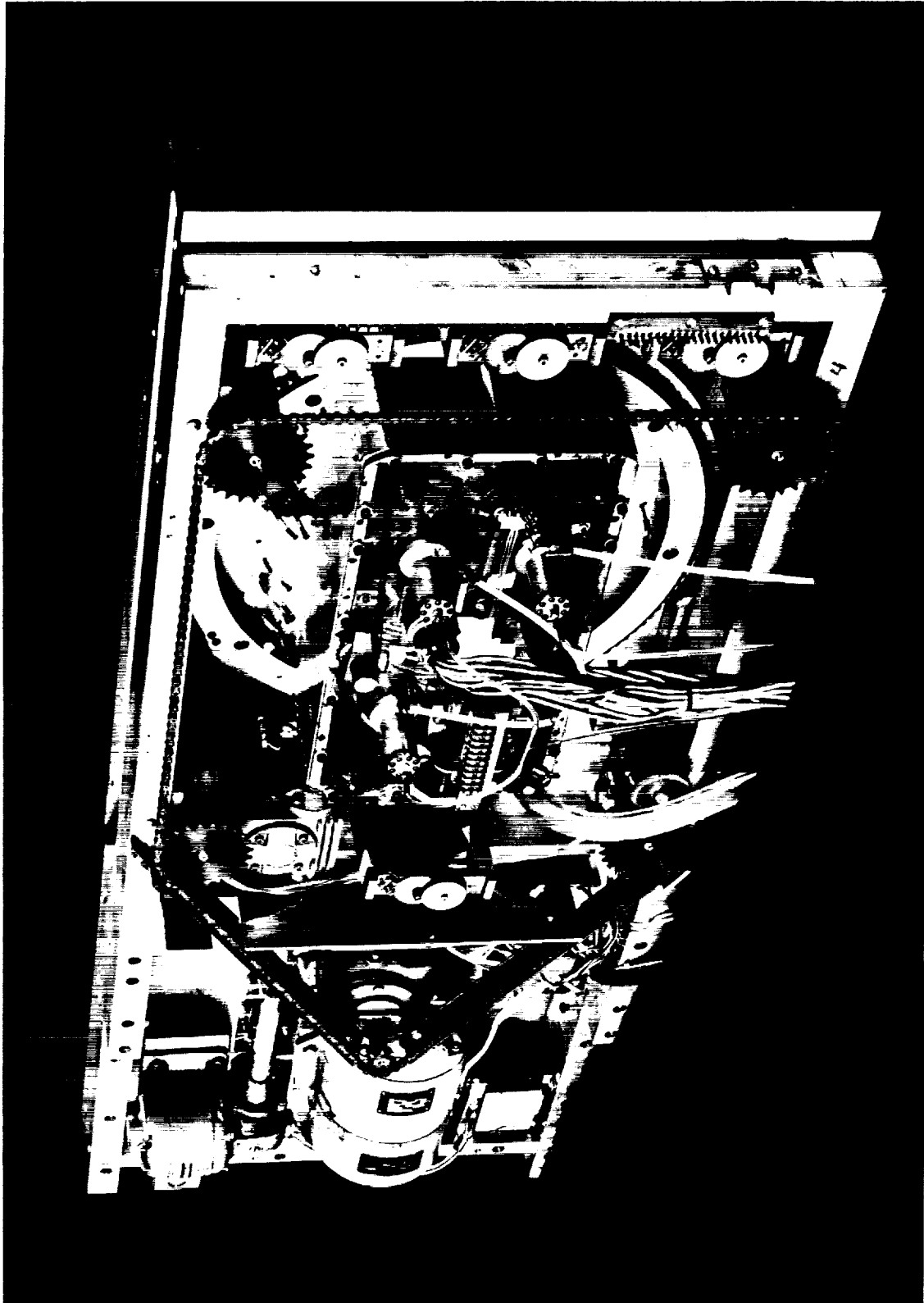


Figure 2.- Layout of variable boundary-layer test fixture showing panel in two test configurations.



(a) Three-fourths front view of airstream side

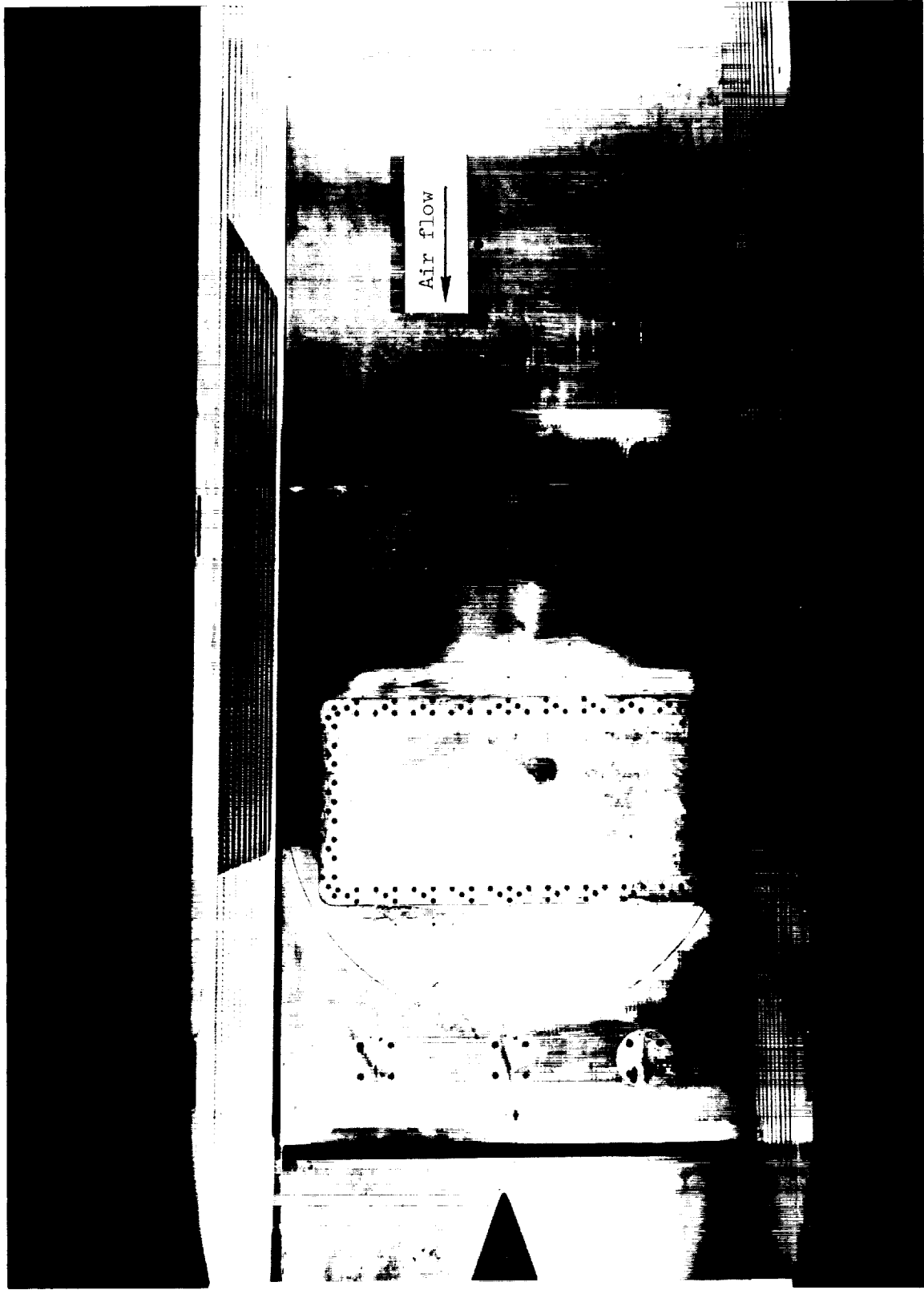
Figure 3.- Variable boundary-layer test fixture.



A-39841

(b) Three-fourths rear view of plenum chamber side

Figure 3.- Concluded.



A-35851

Figure 4.- Panel with variable boundary-layer fixture installed in the 2-by 2-foot transonic wind tunnel.

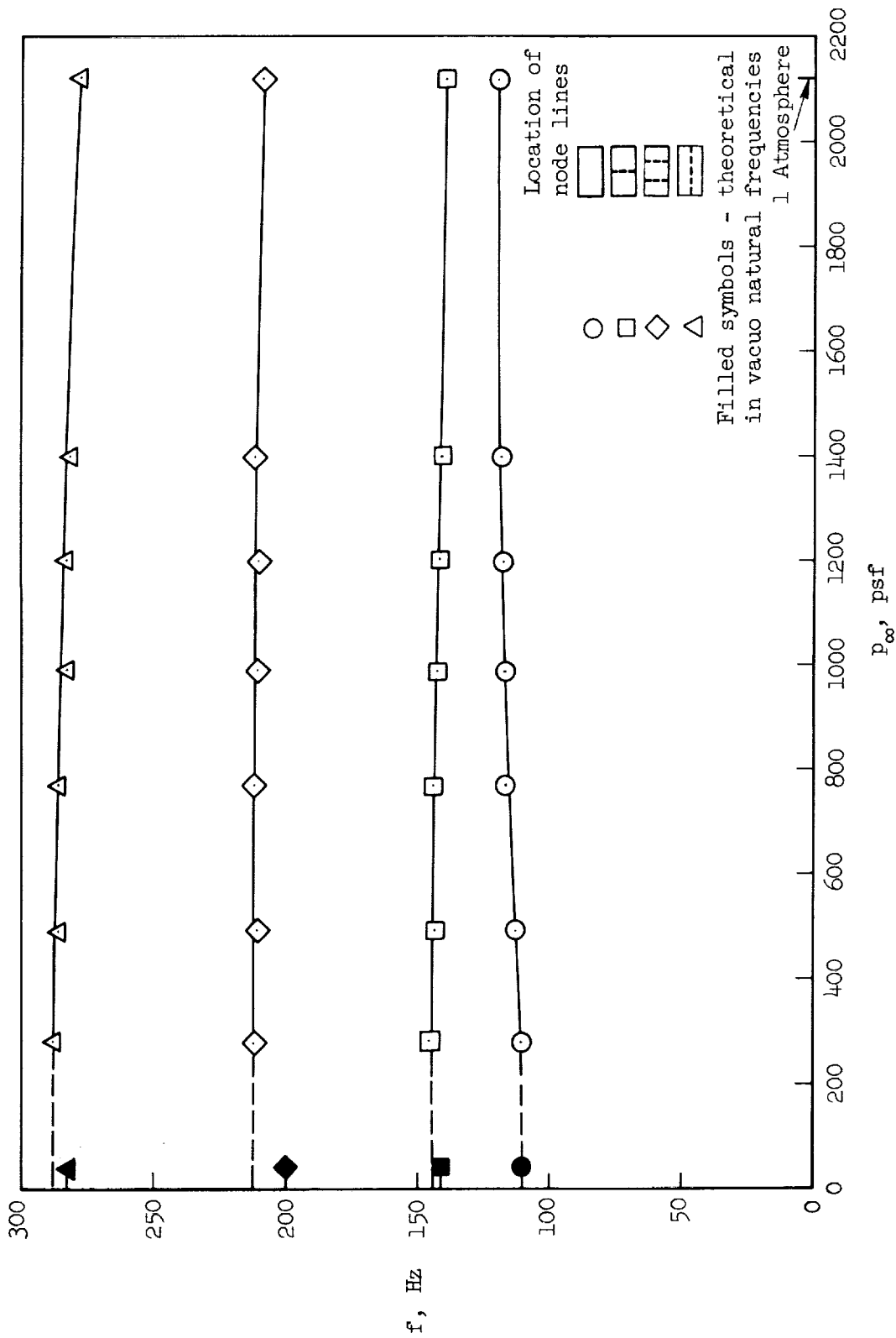


Figure 5.- Effect of static pressure on the natural frequencies of the test panel (cavity depth, 7.5 in.).

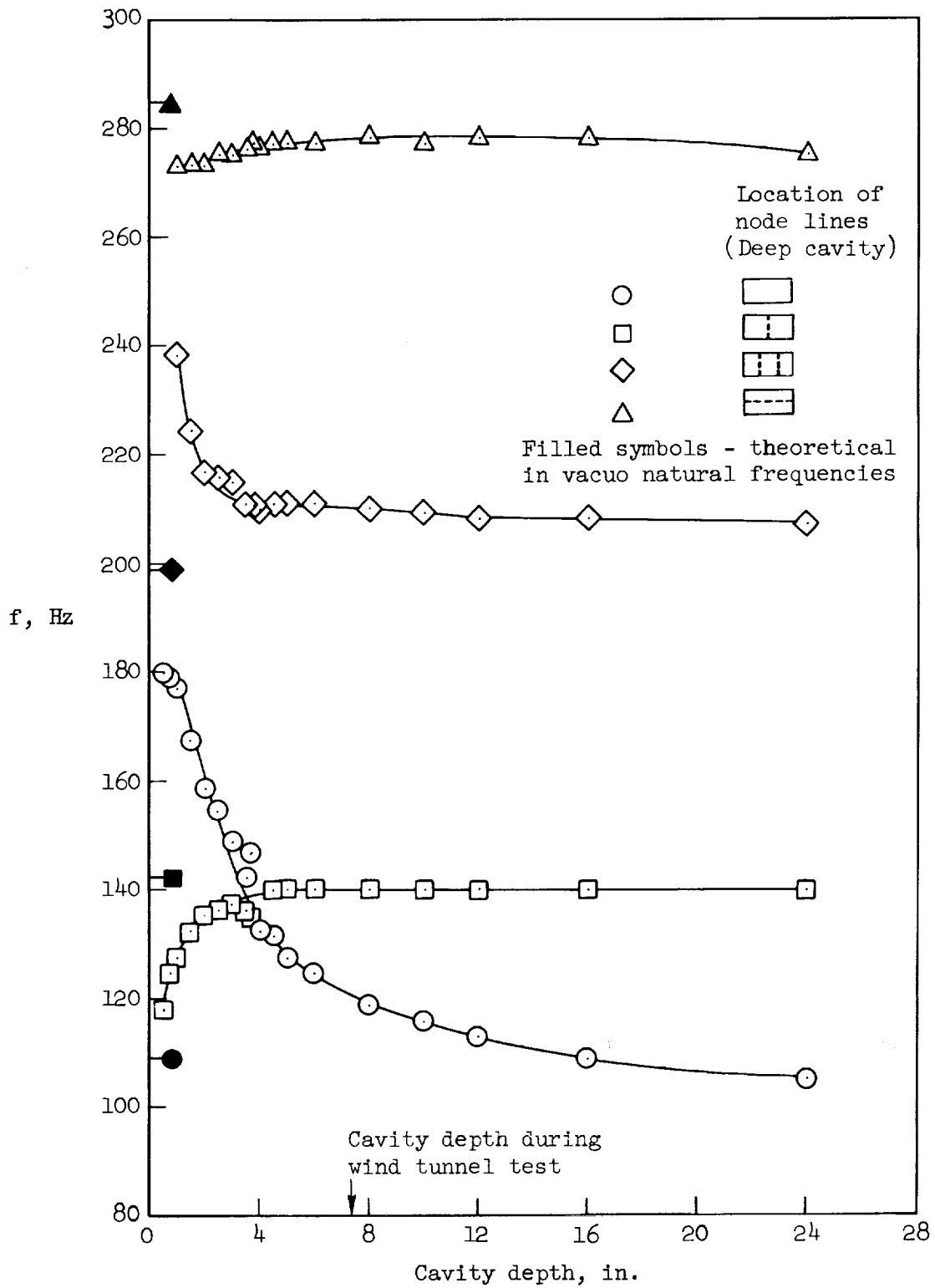


Figure 6.- Effect of cavity depth on panel natural frequencies at atmospheric pressure.

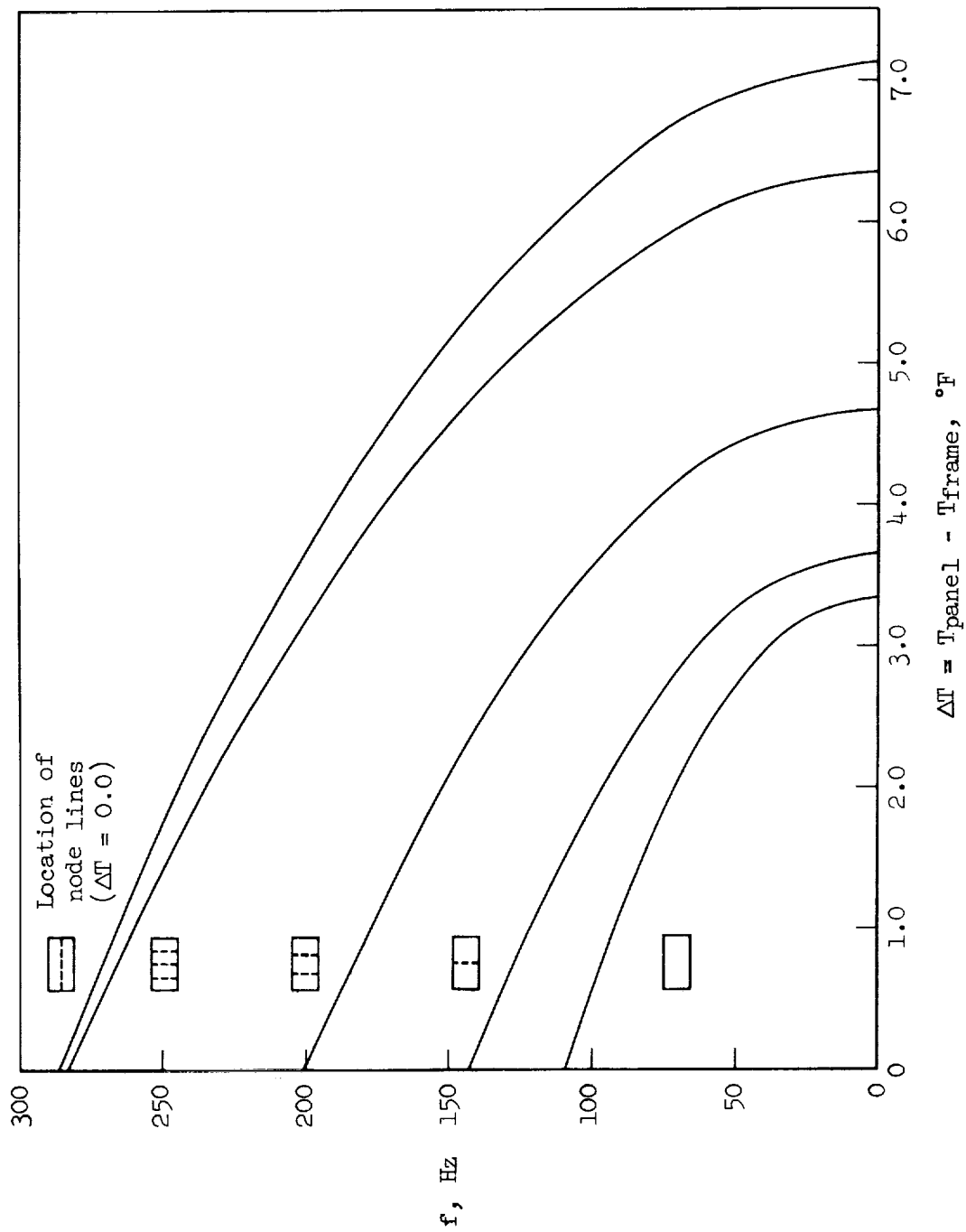


Figure 7.- Theoretical panel natural frequencies as function of differential temperature (no cavity).

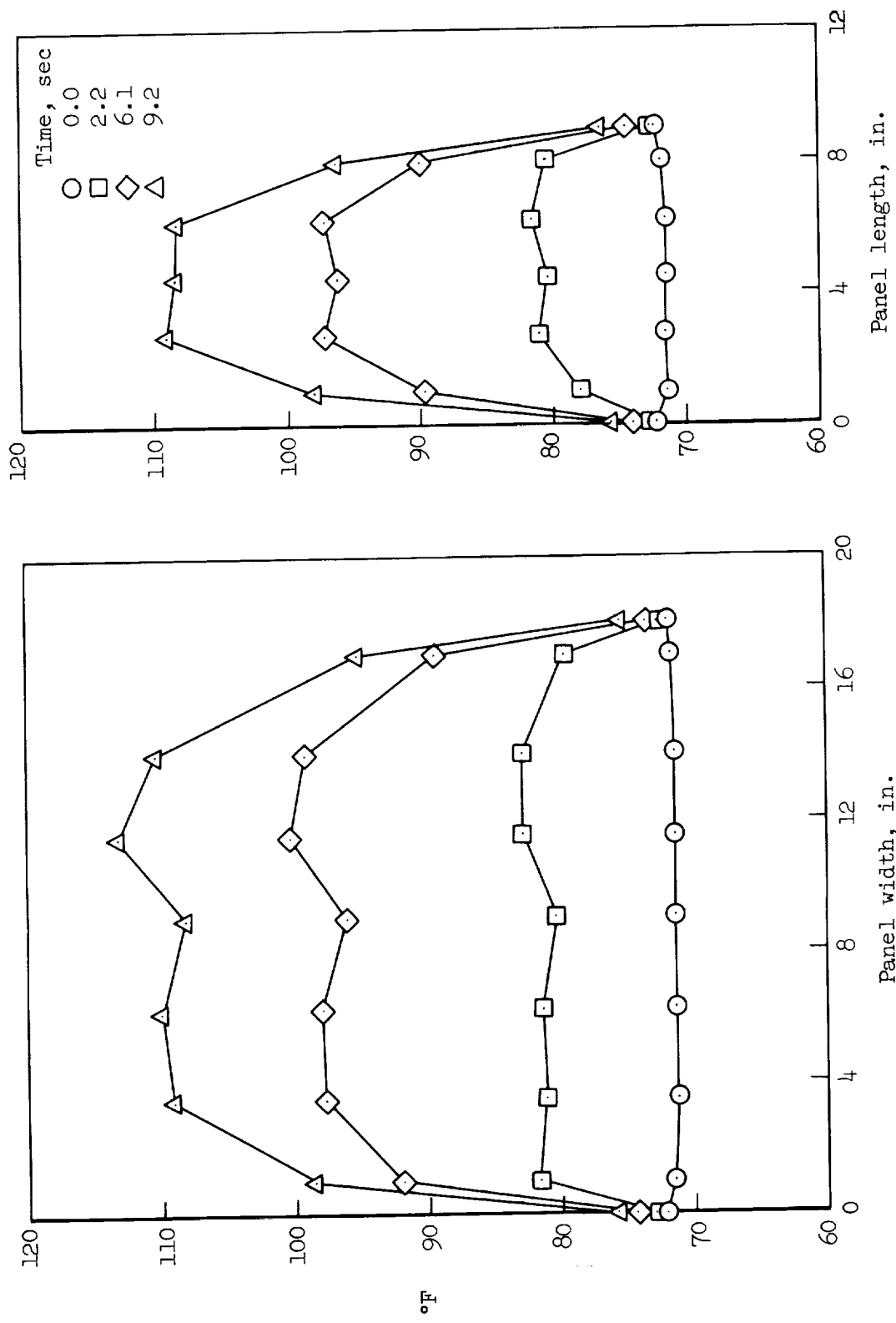


Figure 8.- Typical temperature on unheated side of panel during panel heating test.

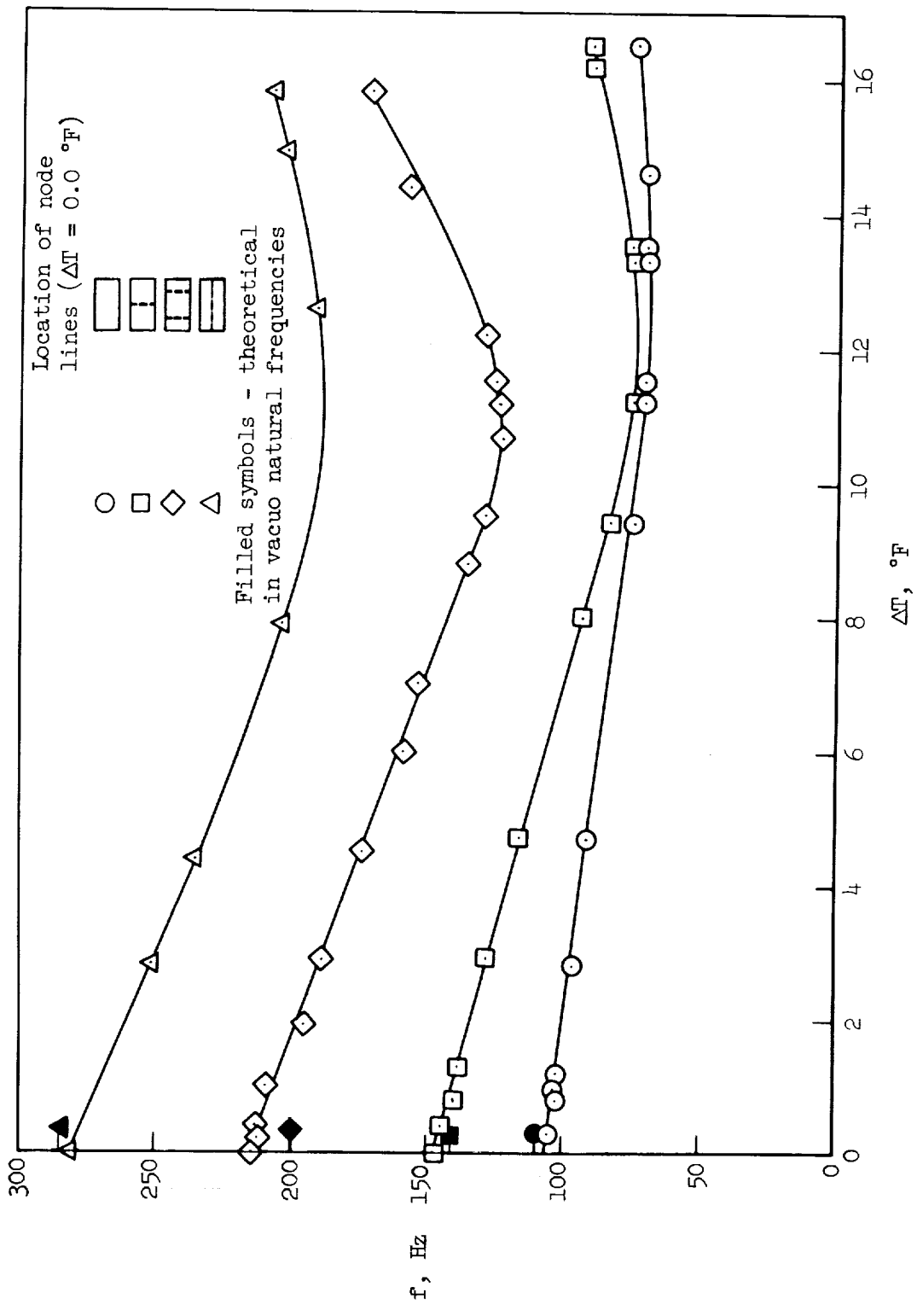


Figure 9.- Experimental panel natural frequencies as a function of differential temperature (no cavity).

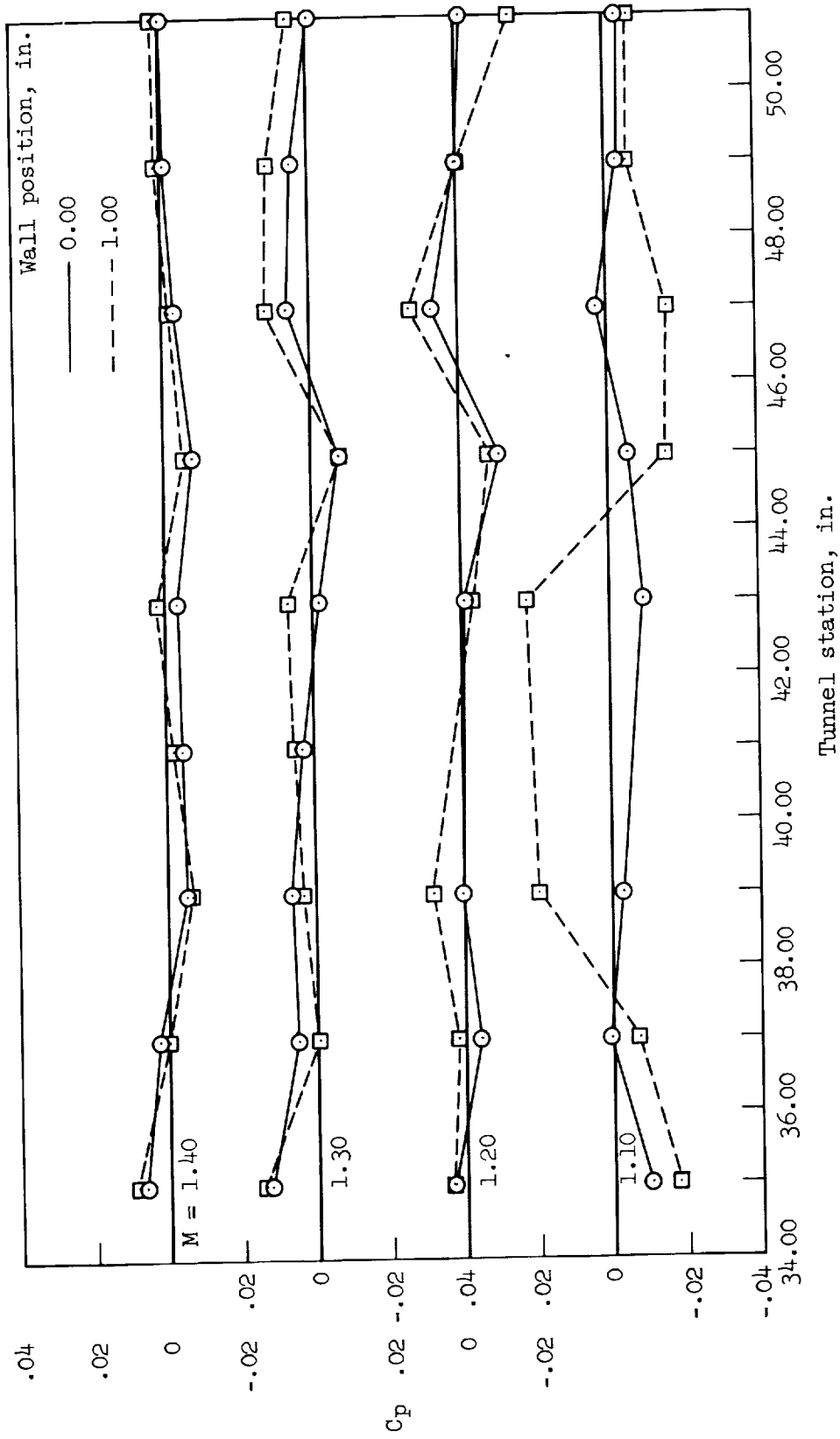


Figure 10.- Typical wall centerline static-pressure distributions in region occupied by panel.

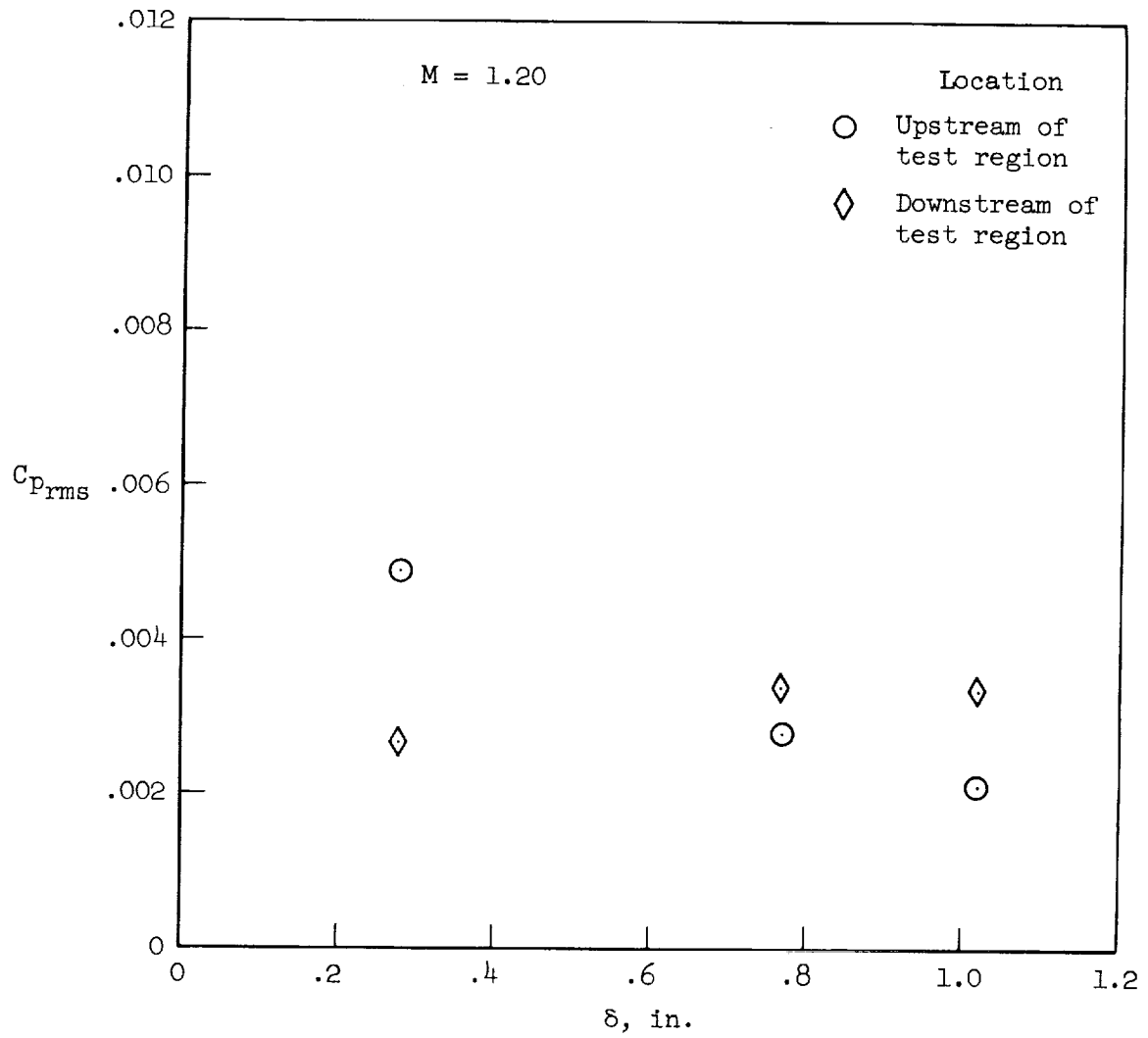


Figure 11.- Typical fluctuating pressure coefficients on wall centerline as a function of boundary-layer thickness.

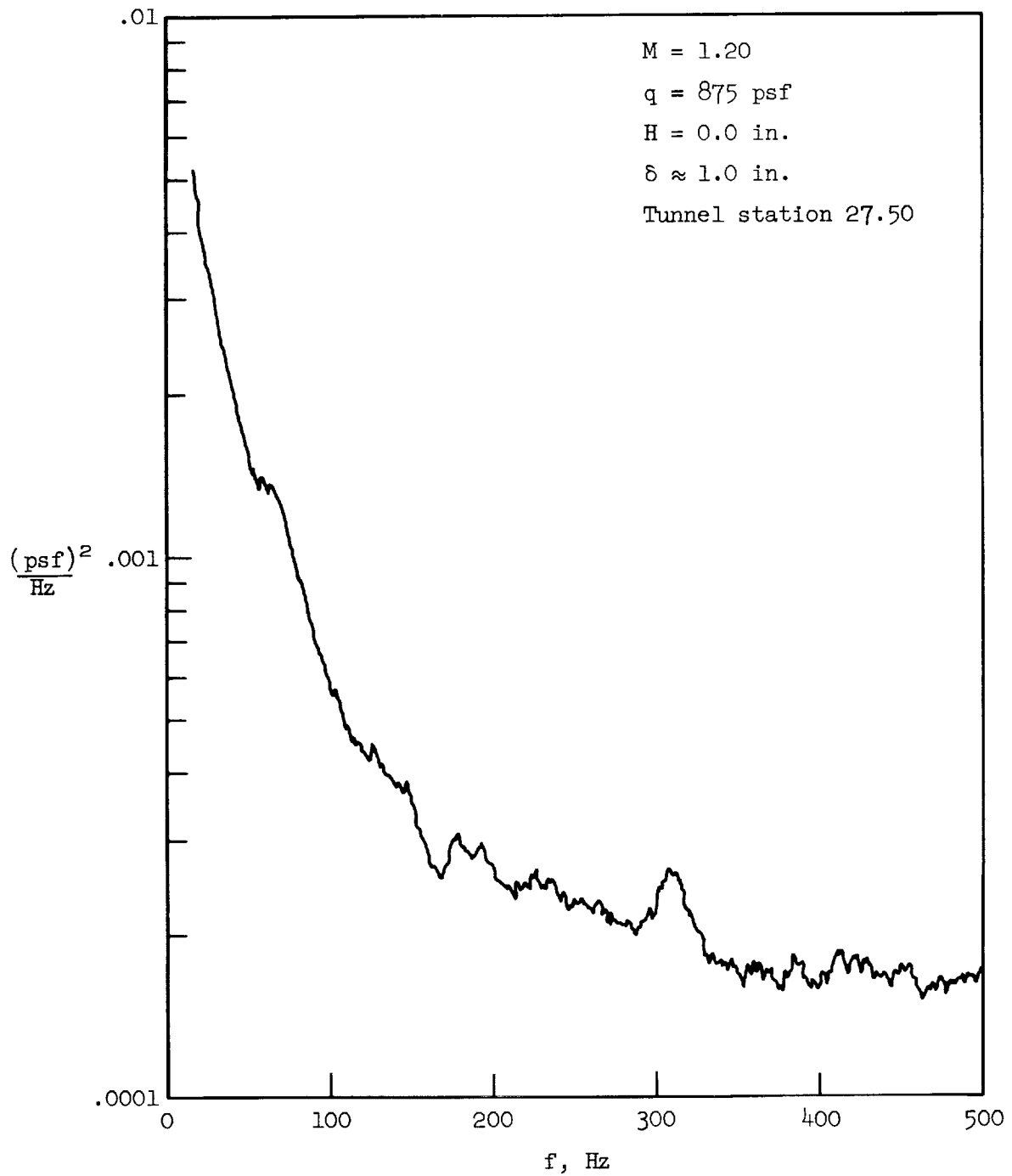


Figure 12.- Typical power spectrum of boundary-layer pressure fluctuations on wall centerline upstream of panel test region.

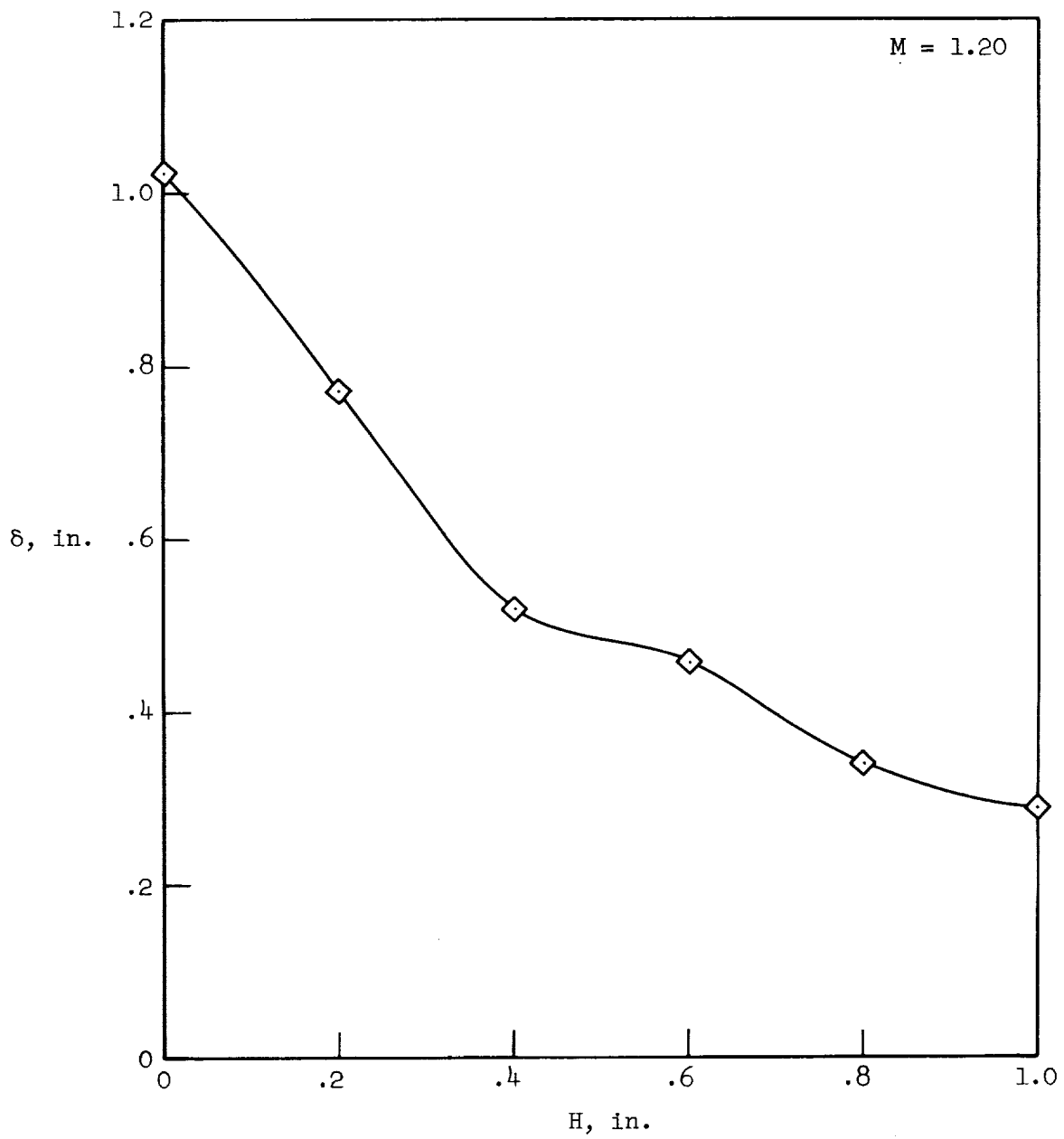
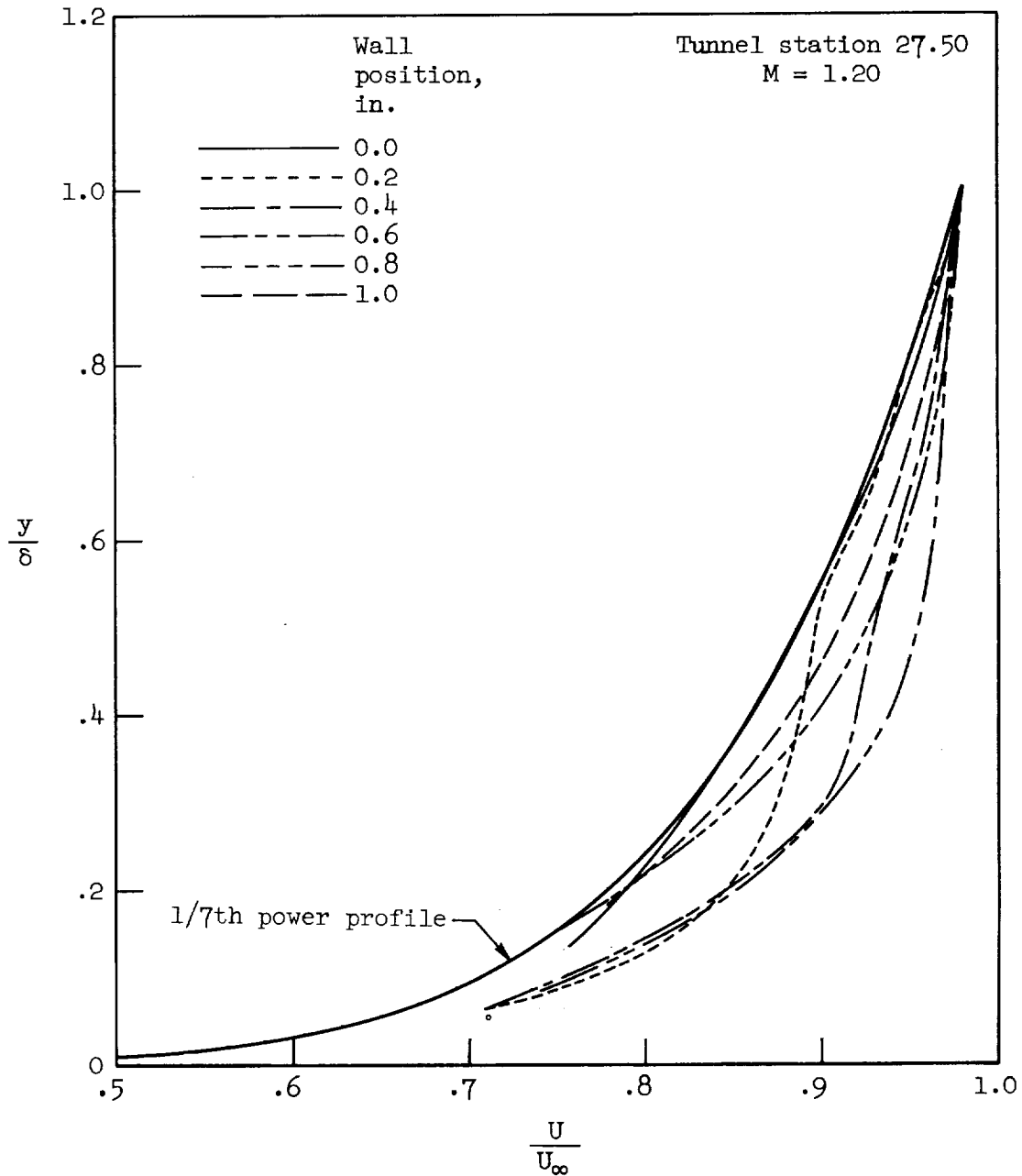
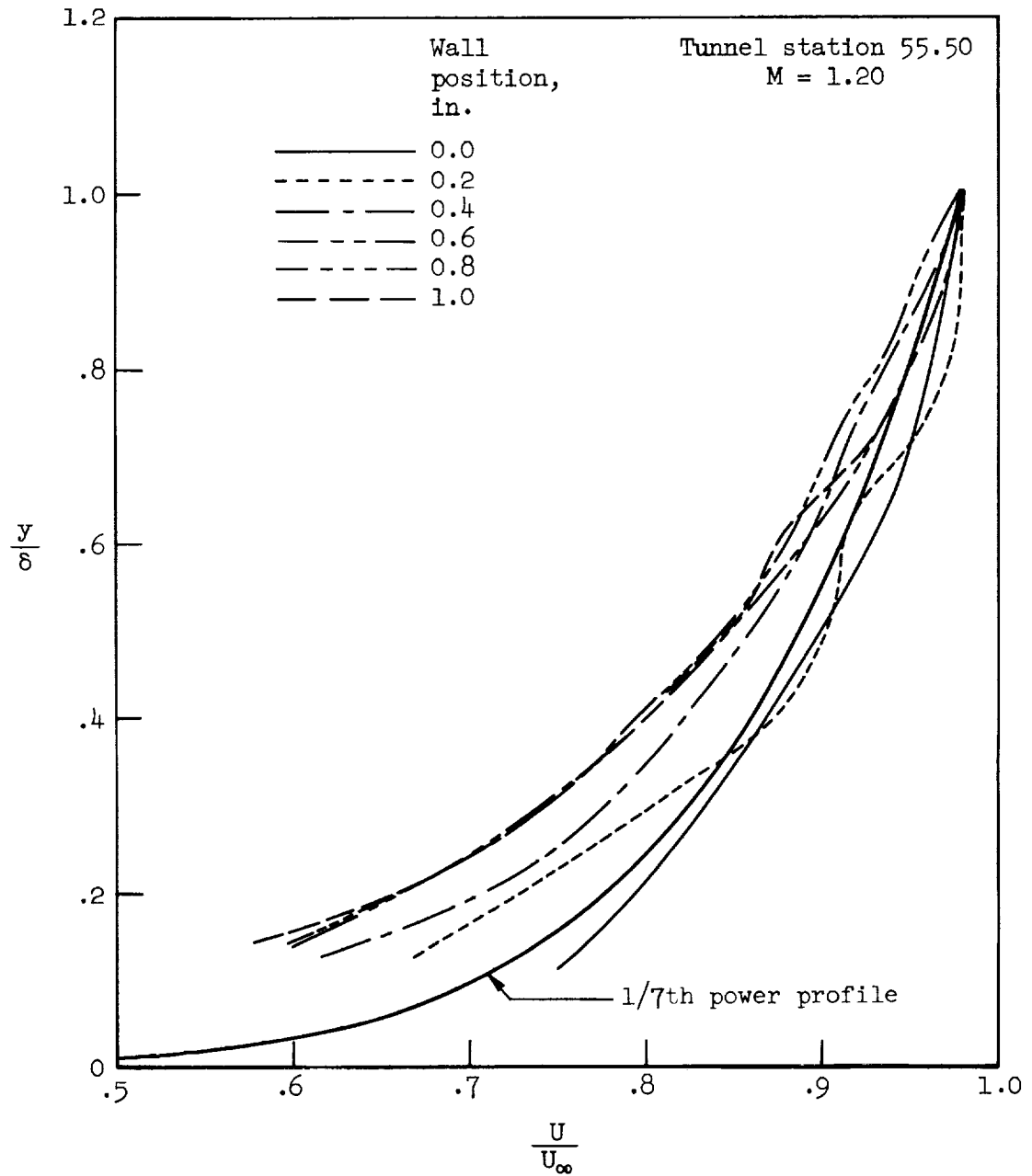


Figure 13.- Typical variation of boundary-layer thickness with wall displacement.



(a) Upstream of panel test region

Figure 14.- Typical normalized boundary-layer velocity profiles on wall centerline.



(b) Downstream of panel test region

Figure 14.- Concluded.

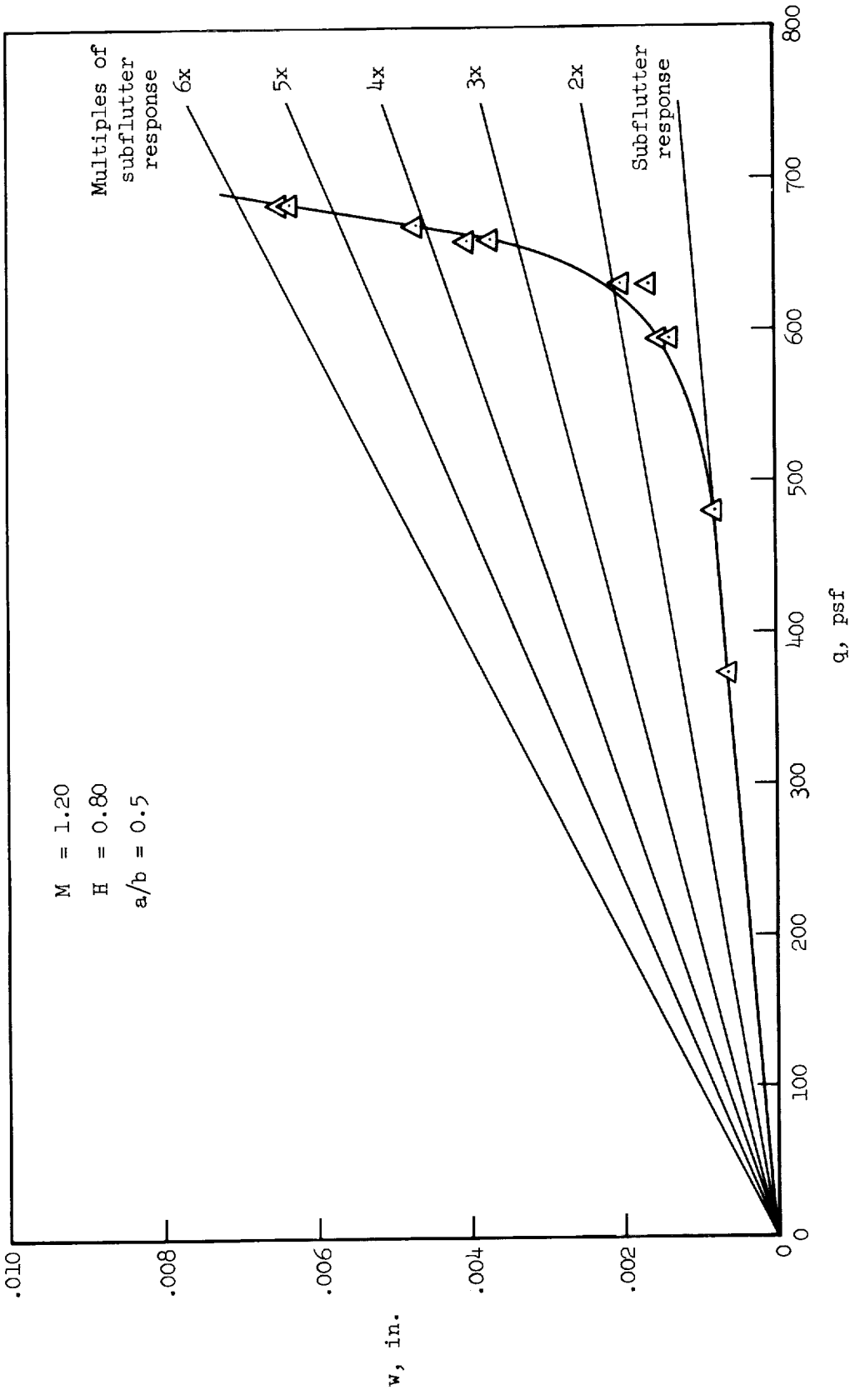


Figure 15.- Typical variation of maximum panel response with dynamic pressure.

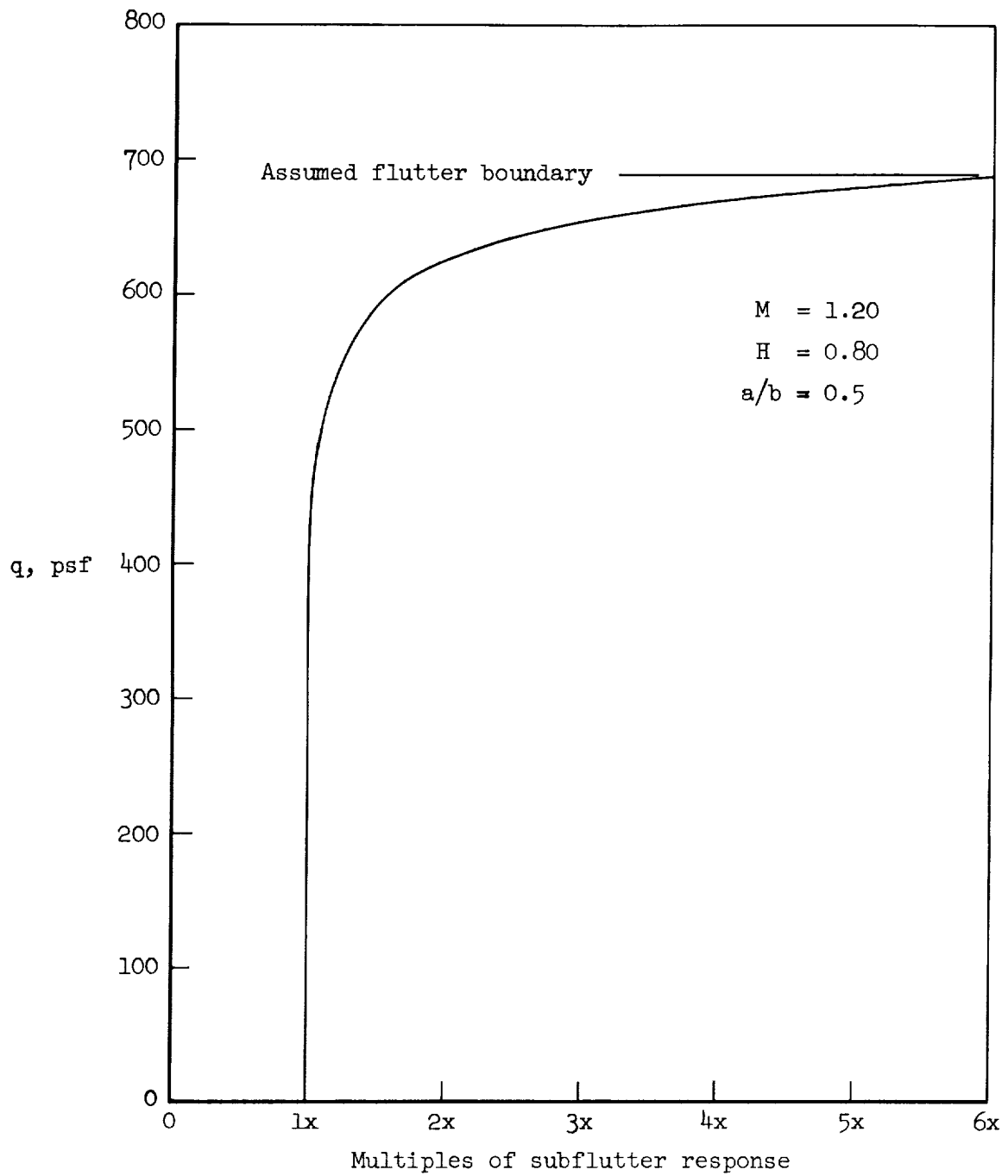


Figure 16.- Typical convergence of multiples of subflutter response with dynamic pressure.

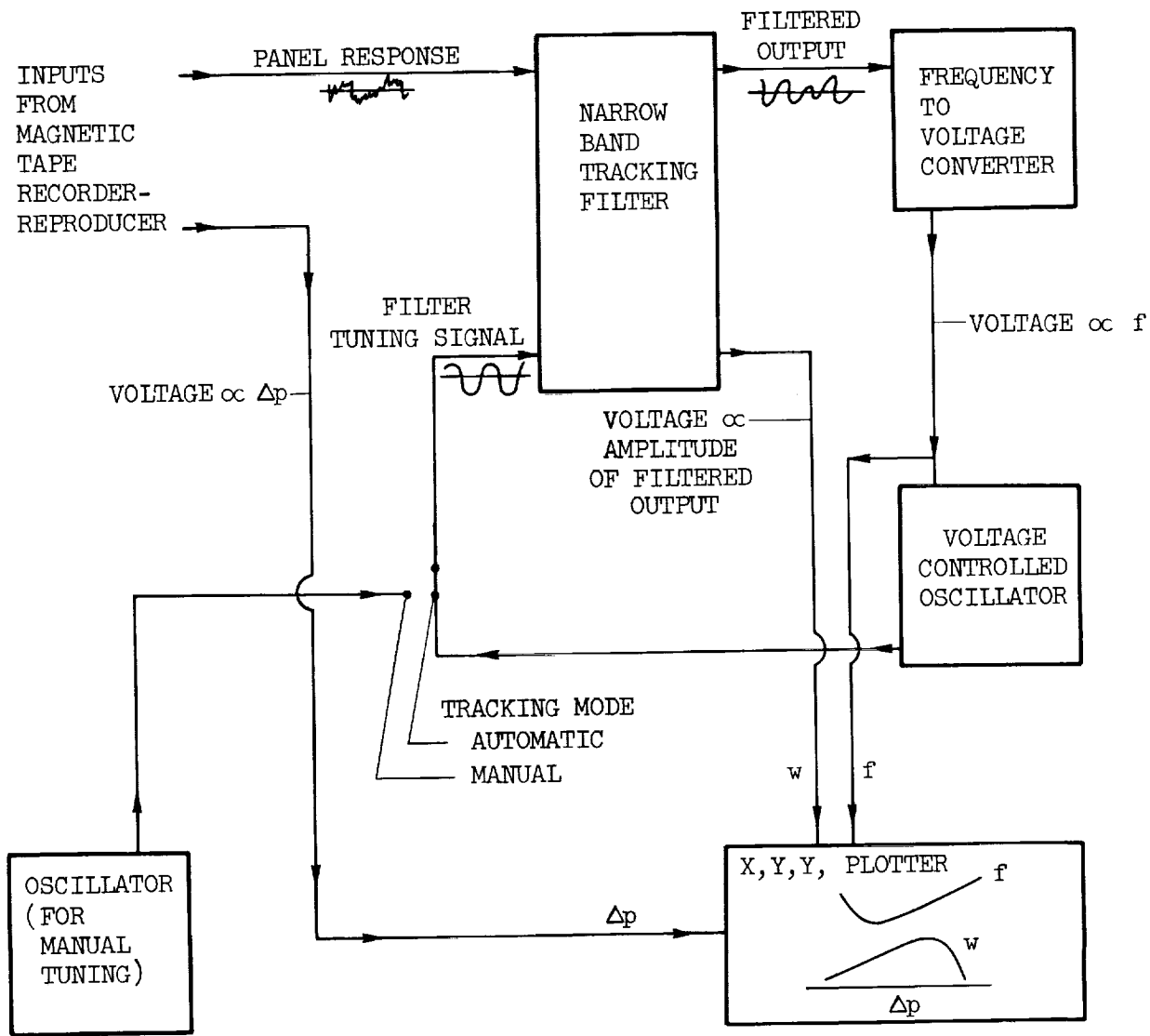


Figure 17.- Block diagram of system used to reduce panel response data.

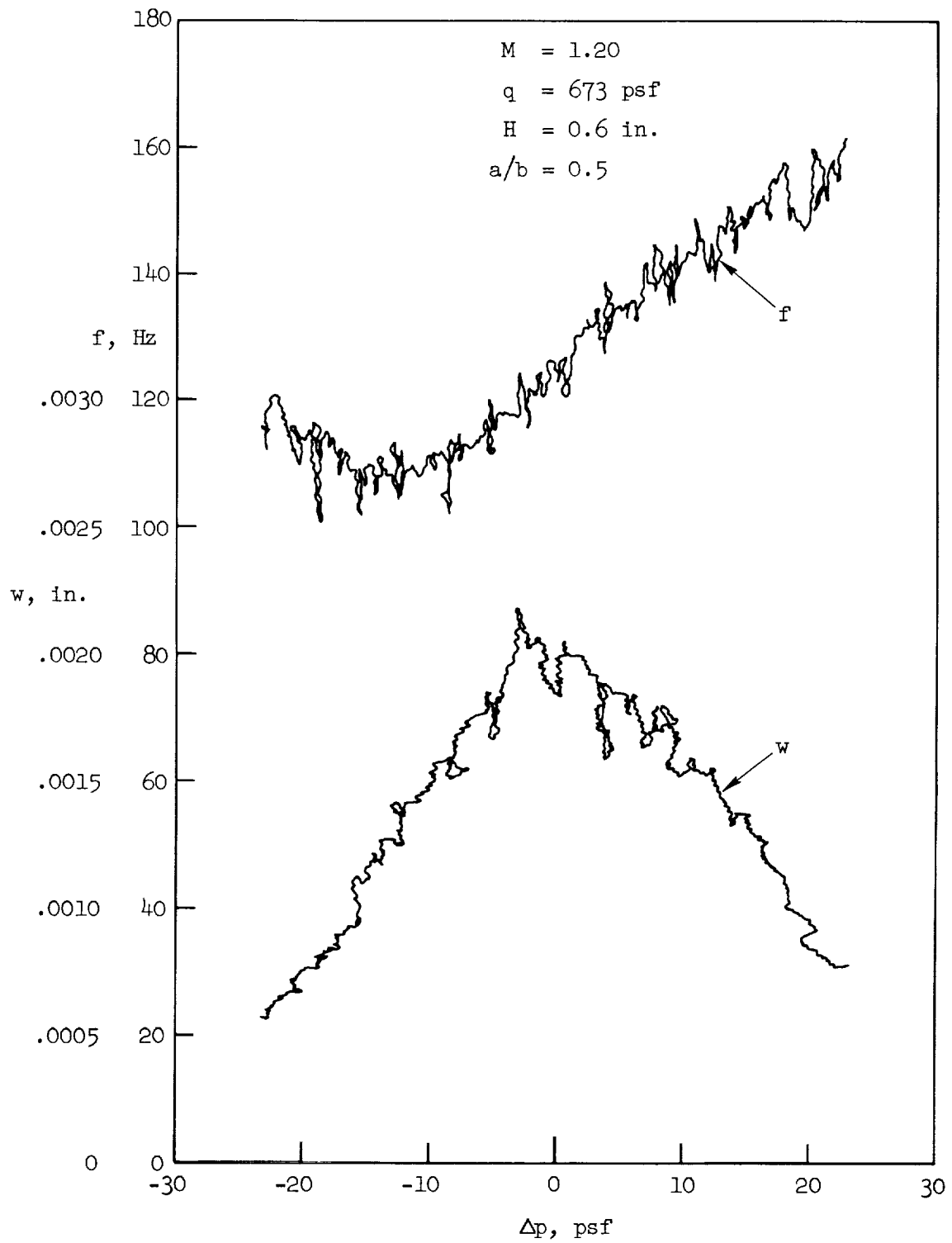


Figure 18.- Typical variation of frequency and amplitude of dominant panel response mode with cavity differential pressure.

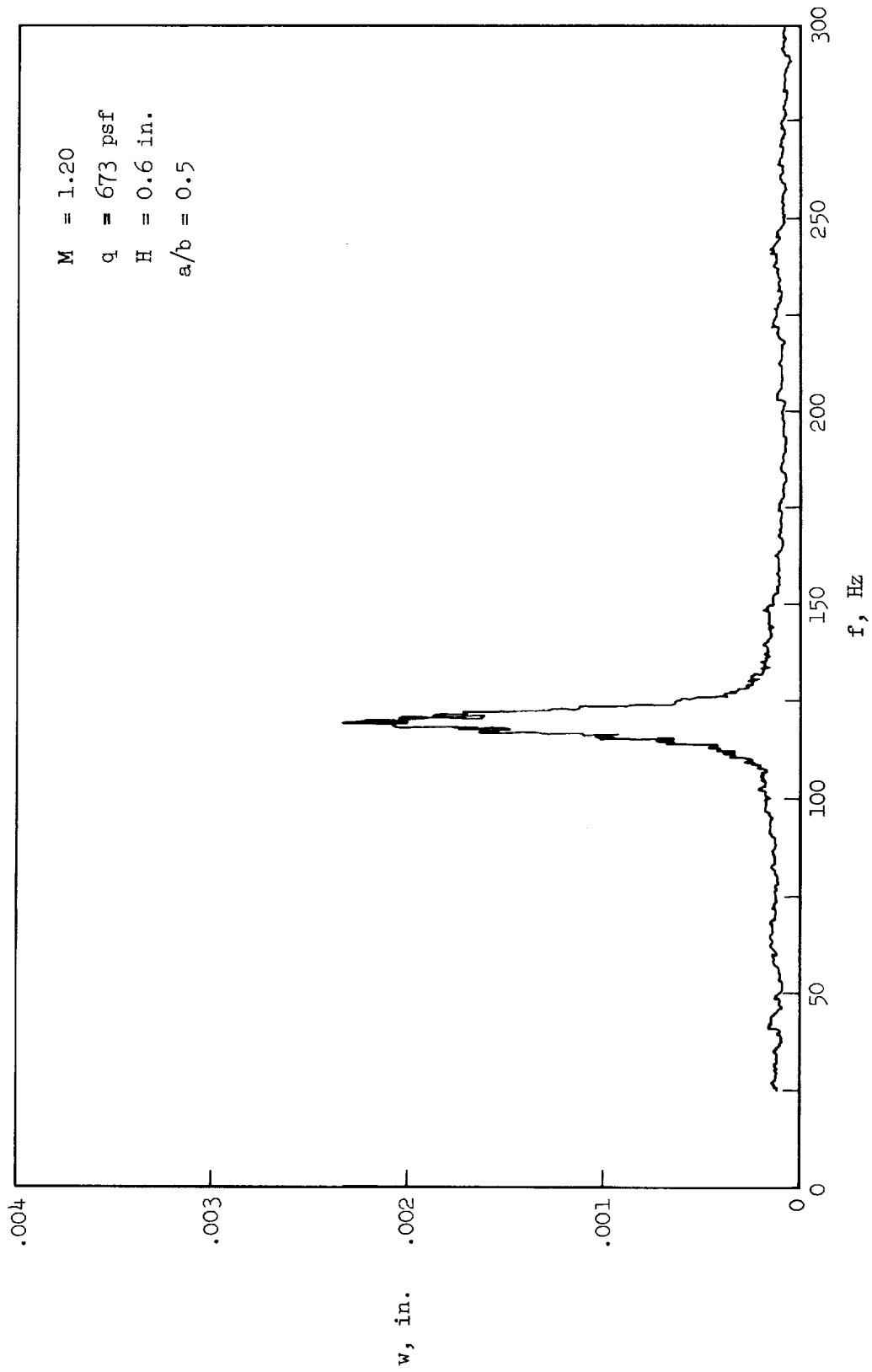


Figure 19.- Typical frequency response spectrum of panel at fixed cavity differential pressure.

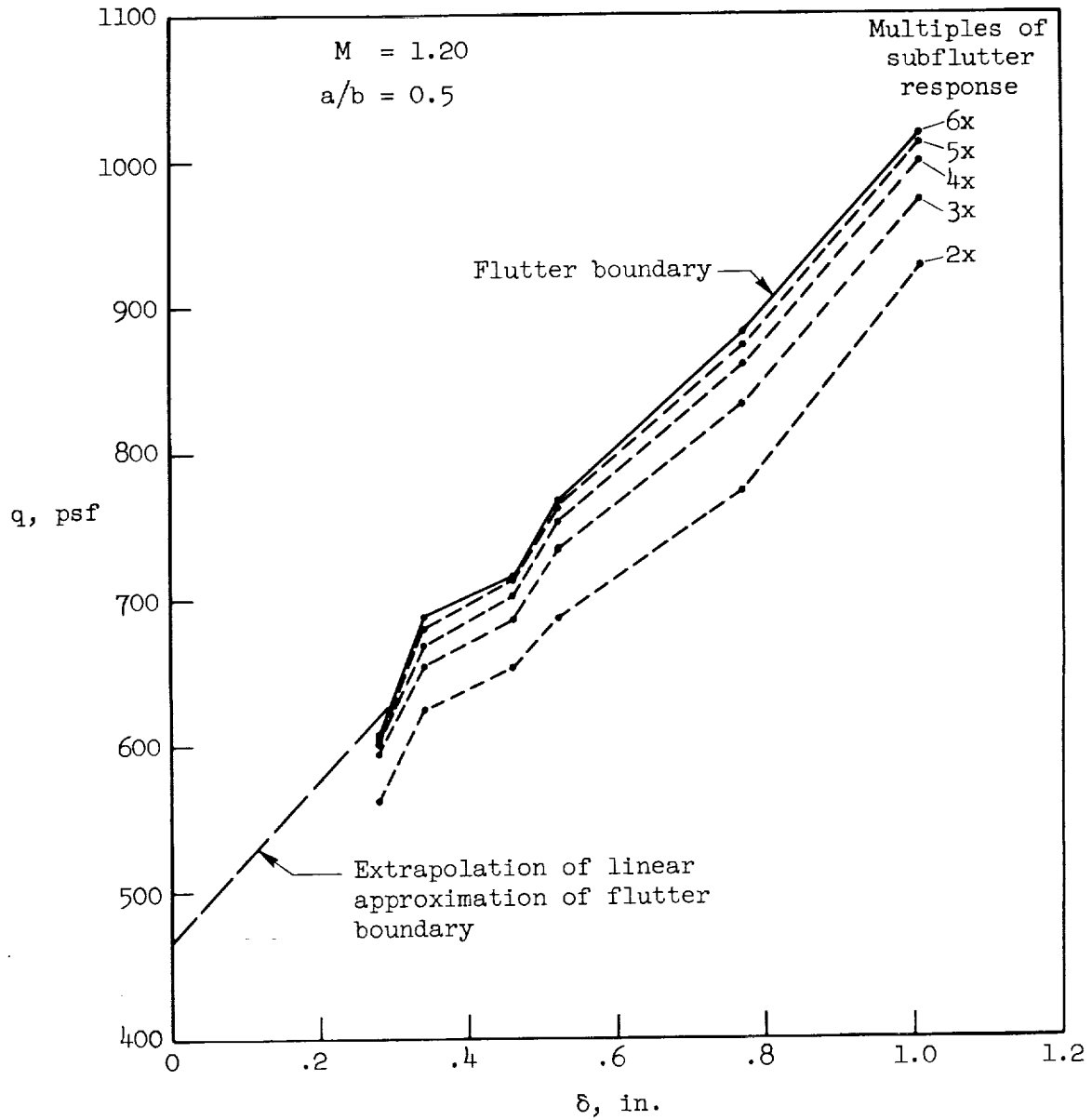


Figure 20.- Dynamic pressure for multiples of subflutter response as a function of boundary-layer thickness for length-to-width ratio of 0.5.

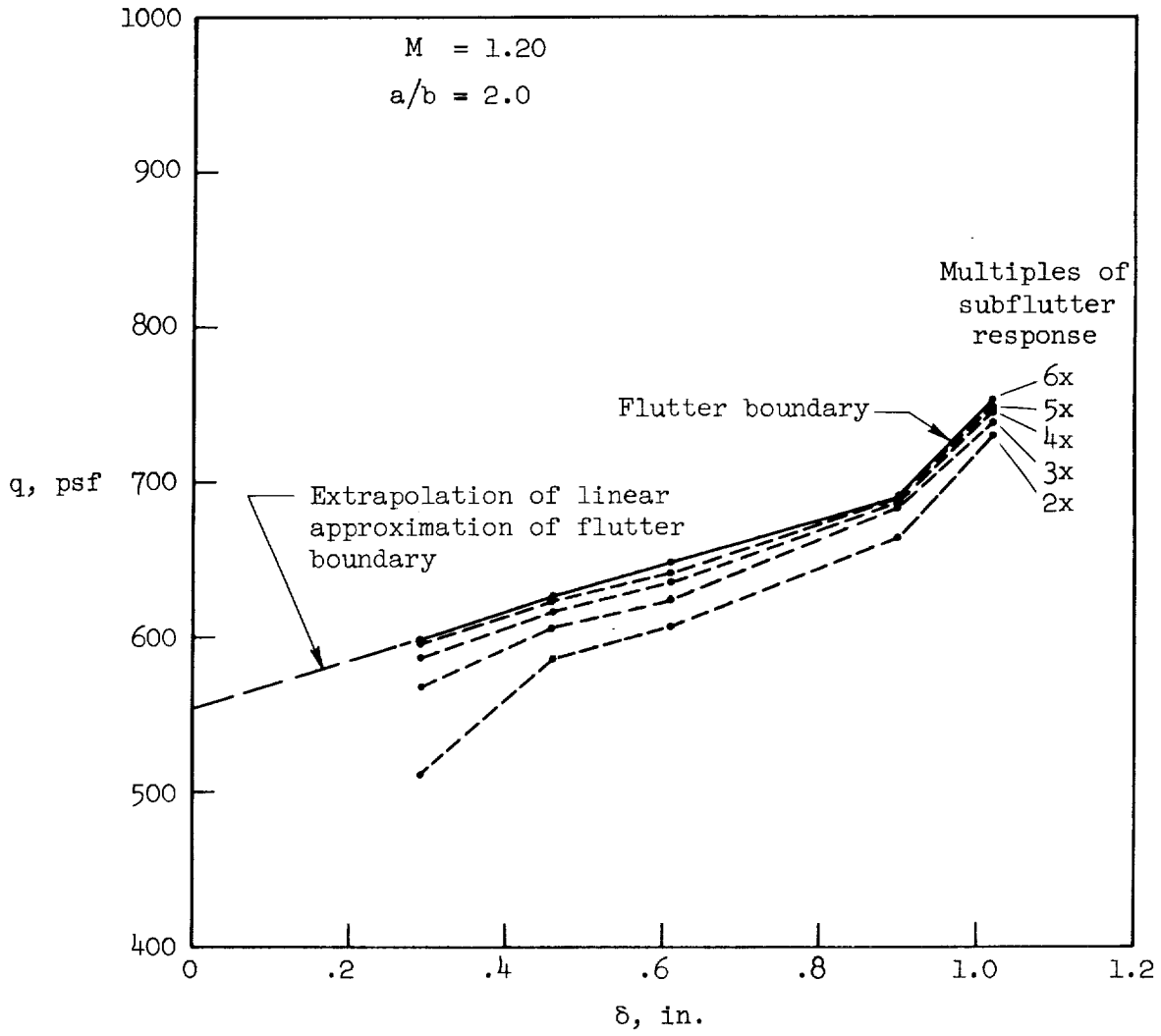


Figure 21.- Dynamic pressure for multiples of subflutter response as a function of boundary-layer thickness for length-to-width ratio of 2.0.

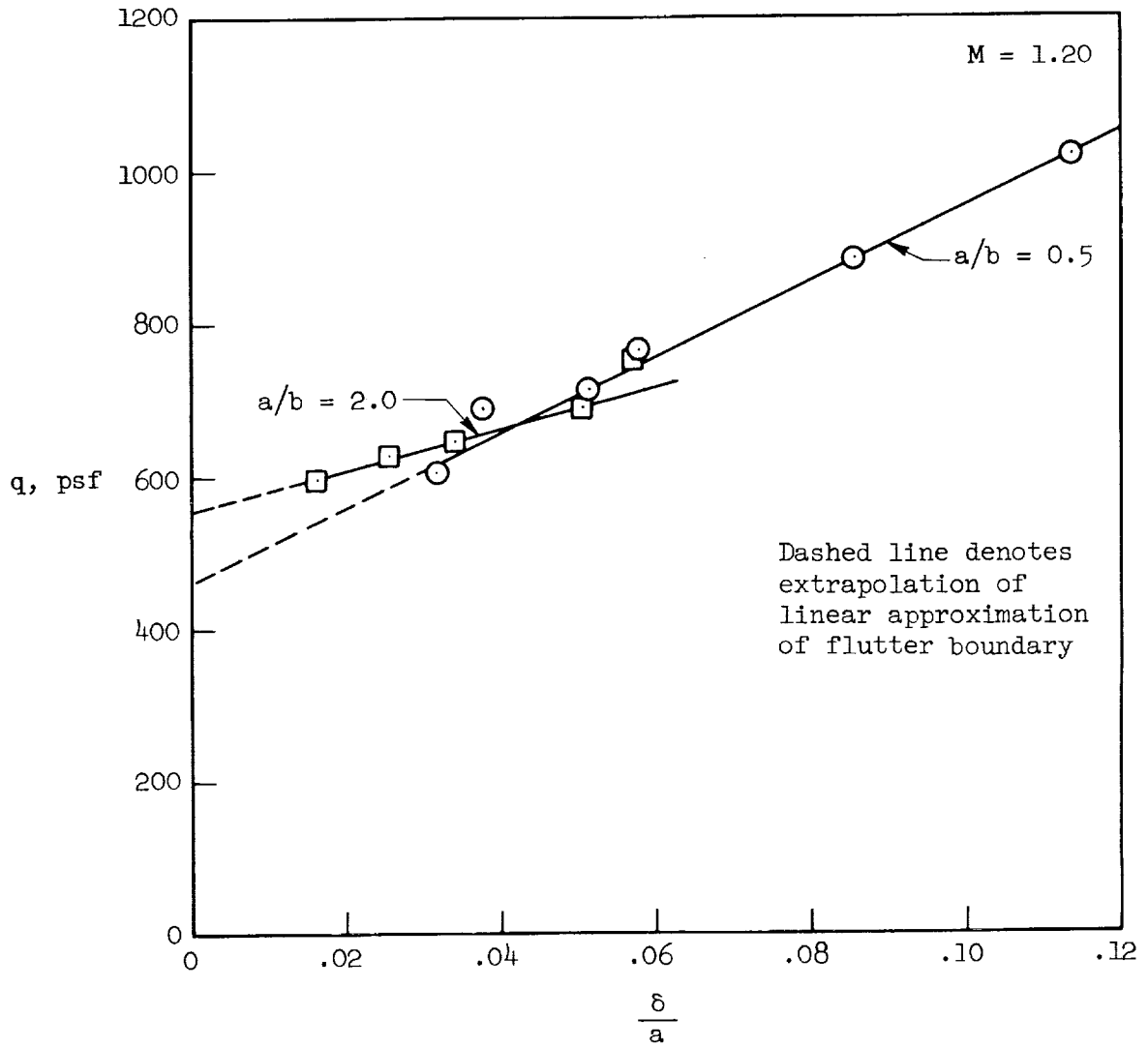


Figure 22.- Flutter dynamic pressure as a function of the ratio of boundary-layer thickness to panel length.

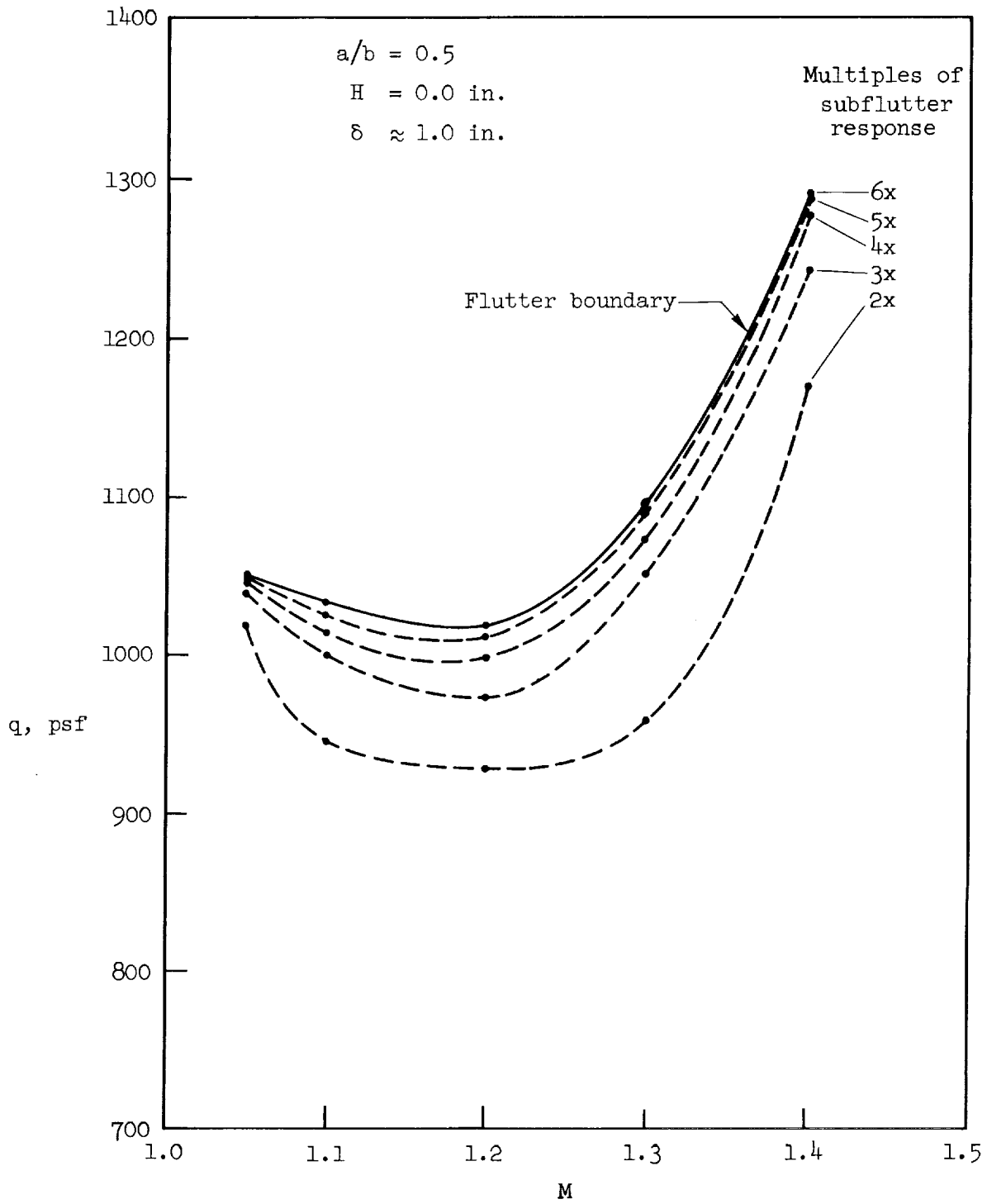


Figure 23.- Dynamic pressure for multiples of subflutter response as a function of Mach number for maximum boundary-layer thickness (approximately 1.0 in.).

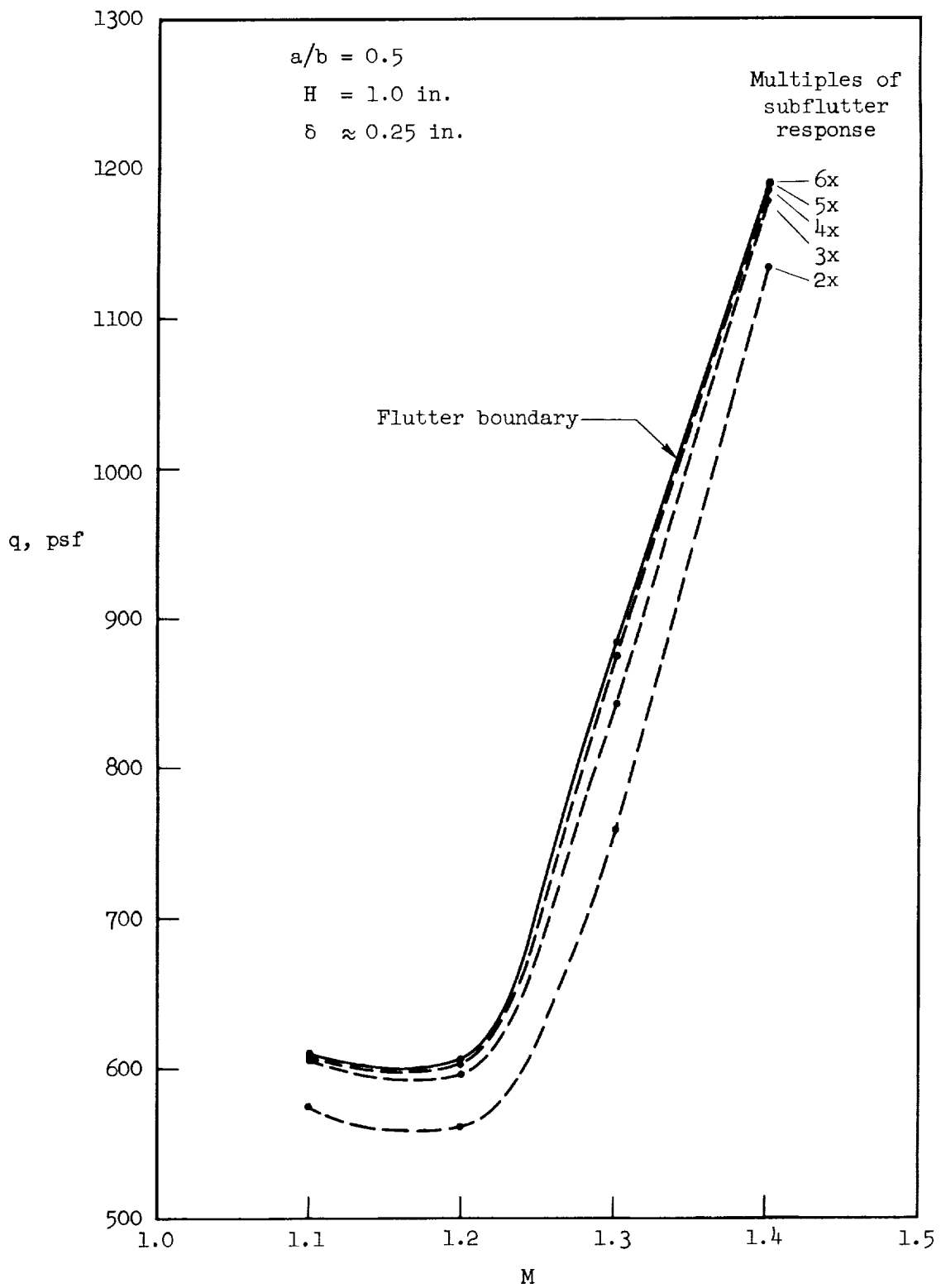


Figure 24.- Dynamic pressure for multiples of subflutter response as a function of Mach number for minimum boundary-layer thickness (approximately 0.25 in.).

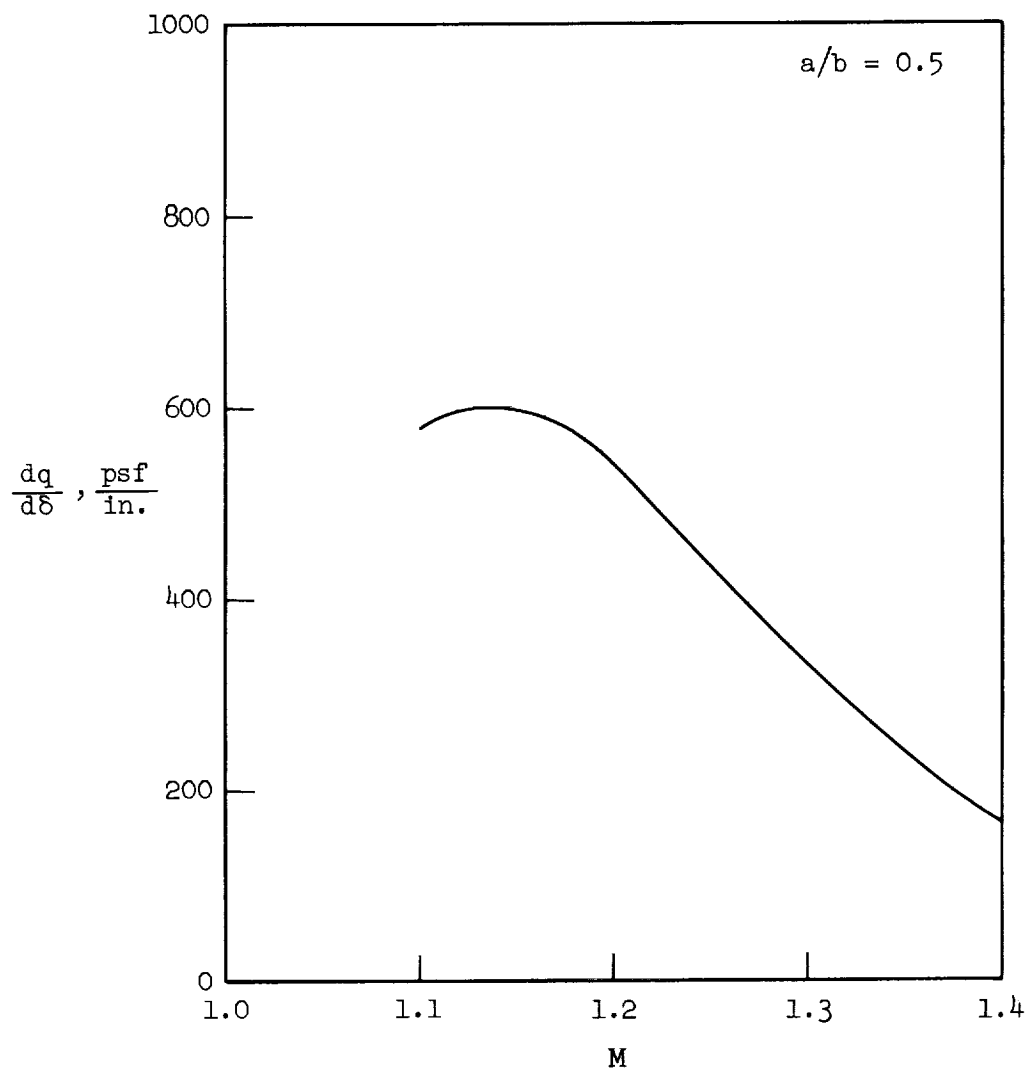


Figure 25.- Rate of change of flutter dynamic pressure with boundary-layer thickness as a function of Mach number.

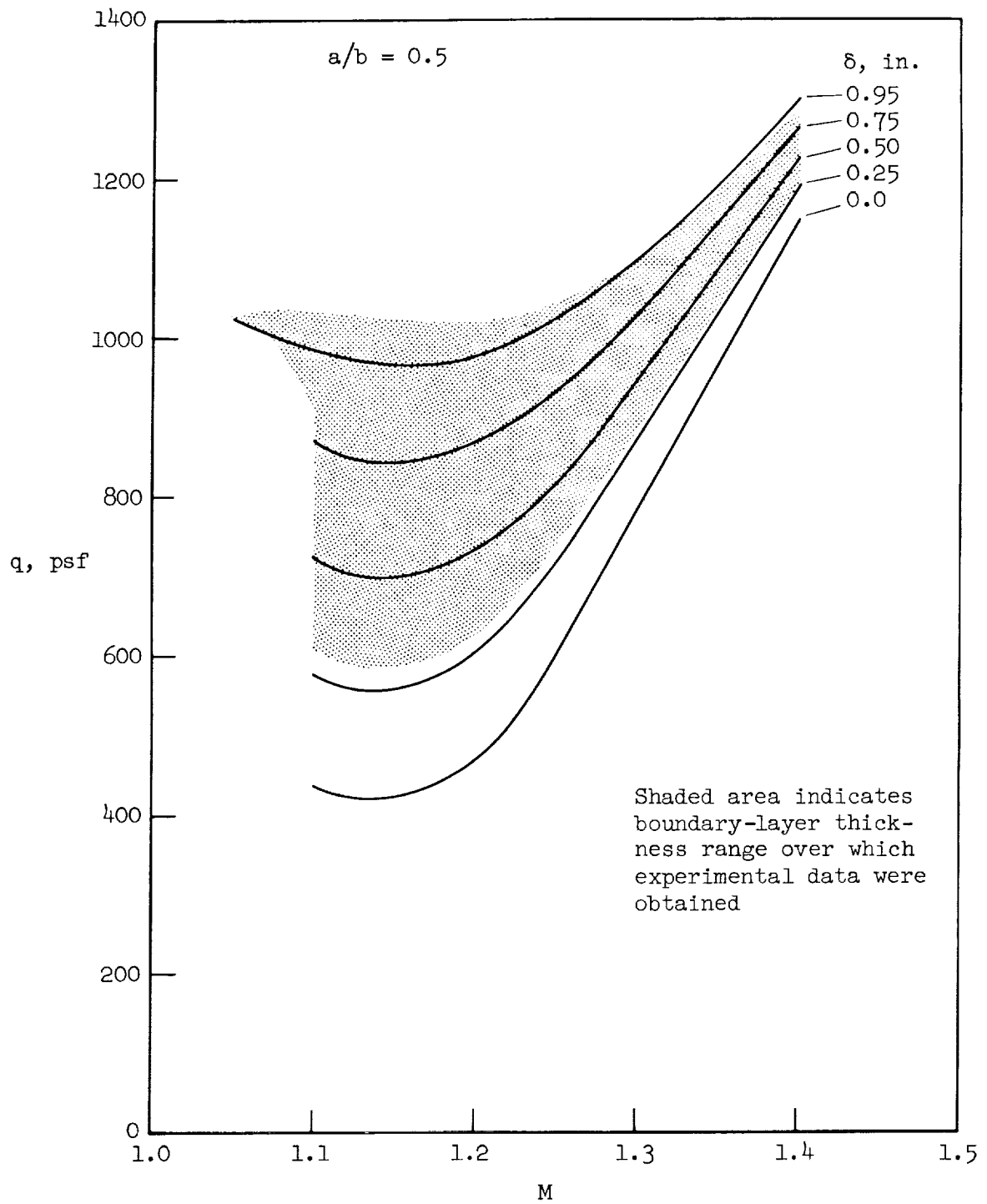


Figure 26.- Flutter dynamic pressure as a function of Mach number derived from linear relationship of flutter dynamic pressure with boundary-layer thickness.

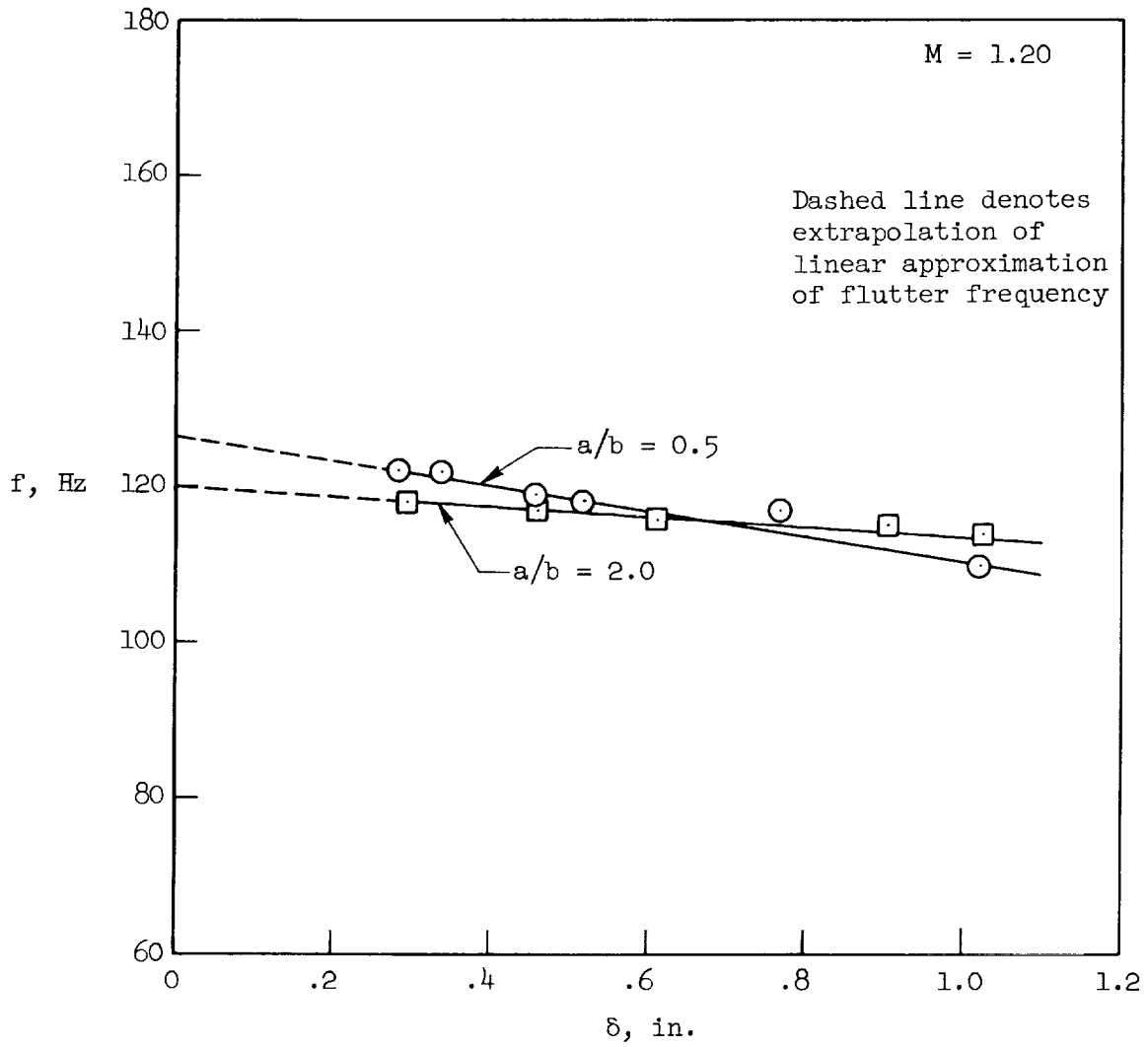


Figure 27.- Flutter frequency as a function of boundary-layer thickness for length-to-width ratios of 0.5 and 2.0.

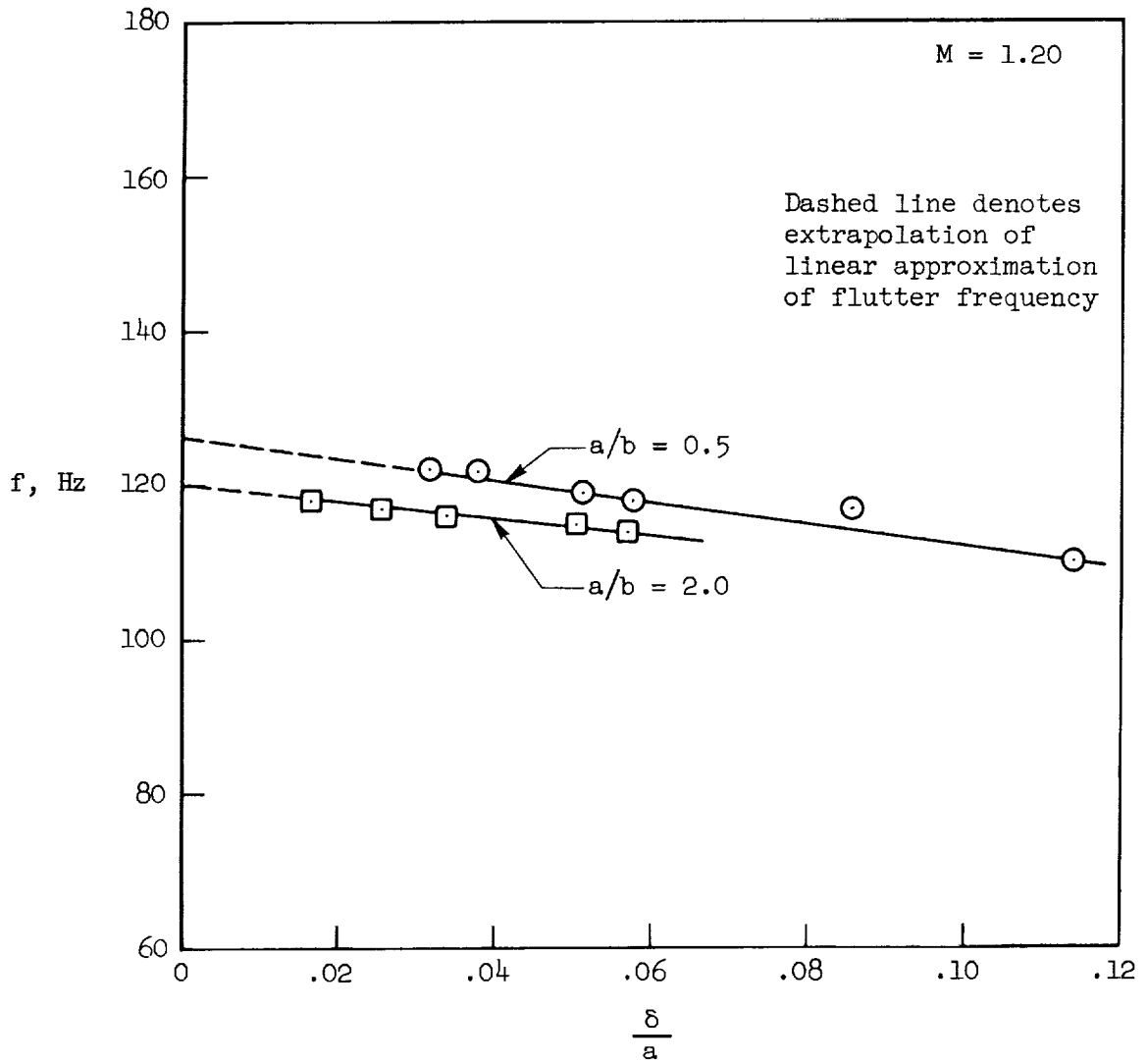


Figure 28.- Flutter frequency as a function of the ratio of boundary-layer thickness to panel length.

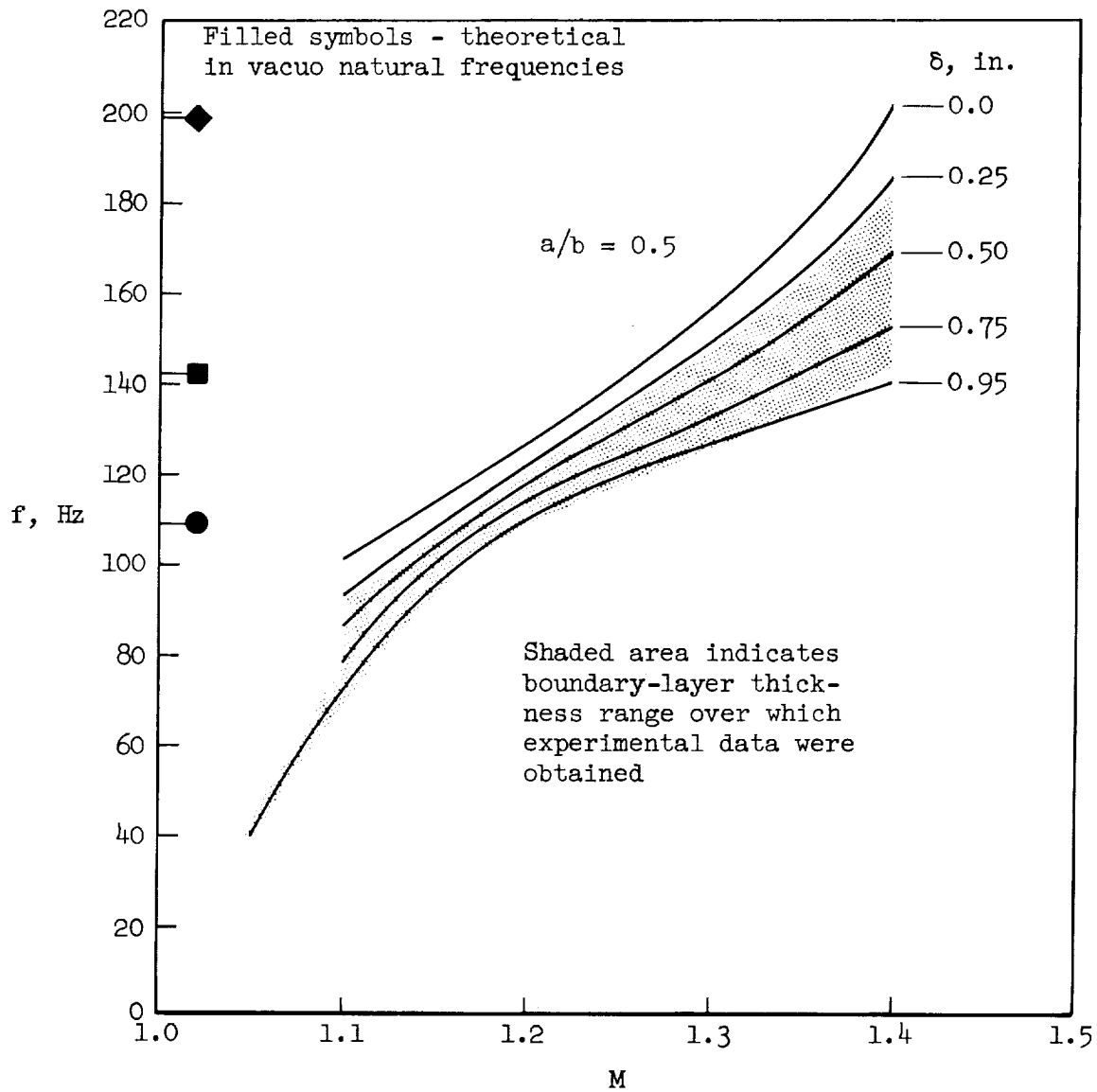


Figure 29.- Flutter frequency as a function of Mach number derived from linear relationship of flutter frequency with boundary-layer thickness.

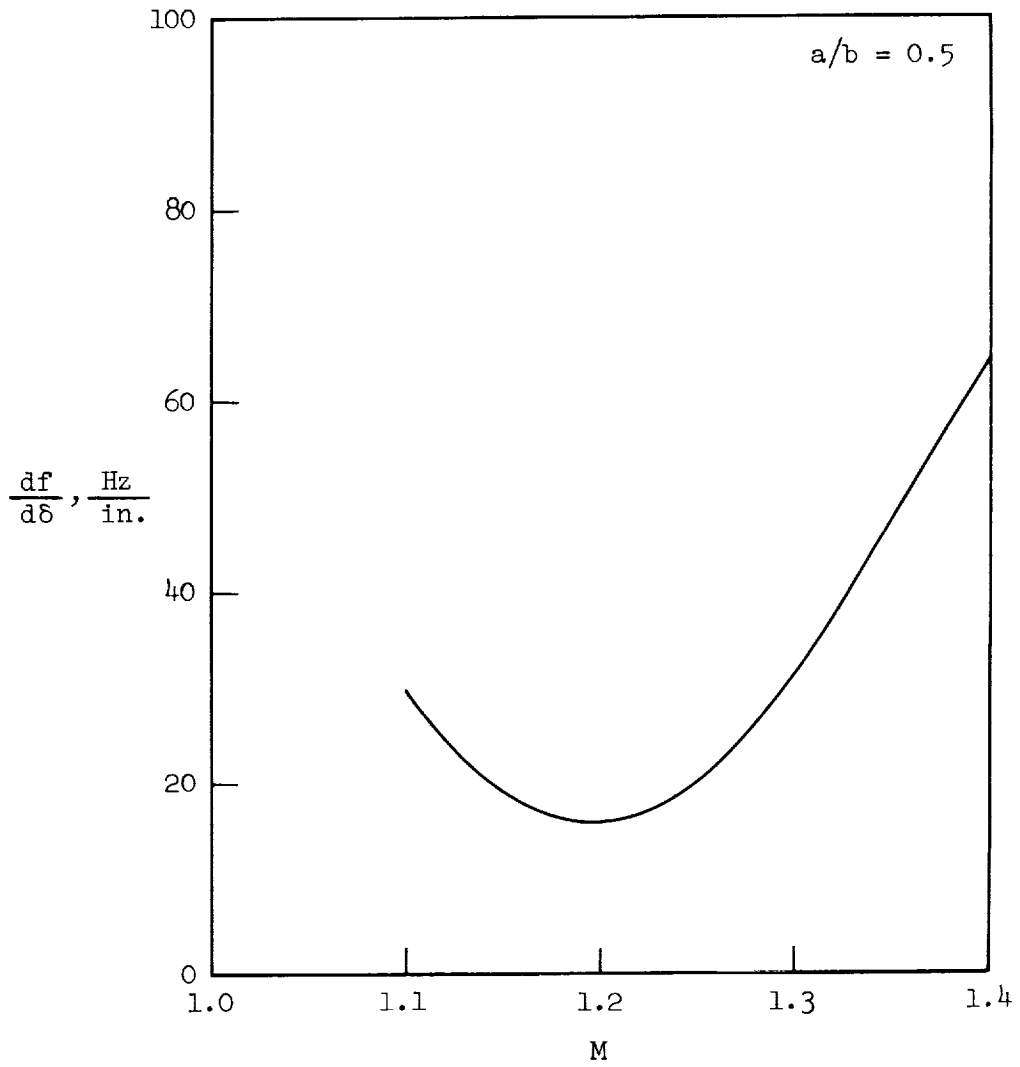


Figure 30.- Rate of change of flutter frequency with boundary-layer thickness as a function of Mach number.

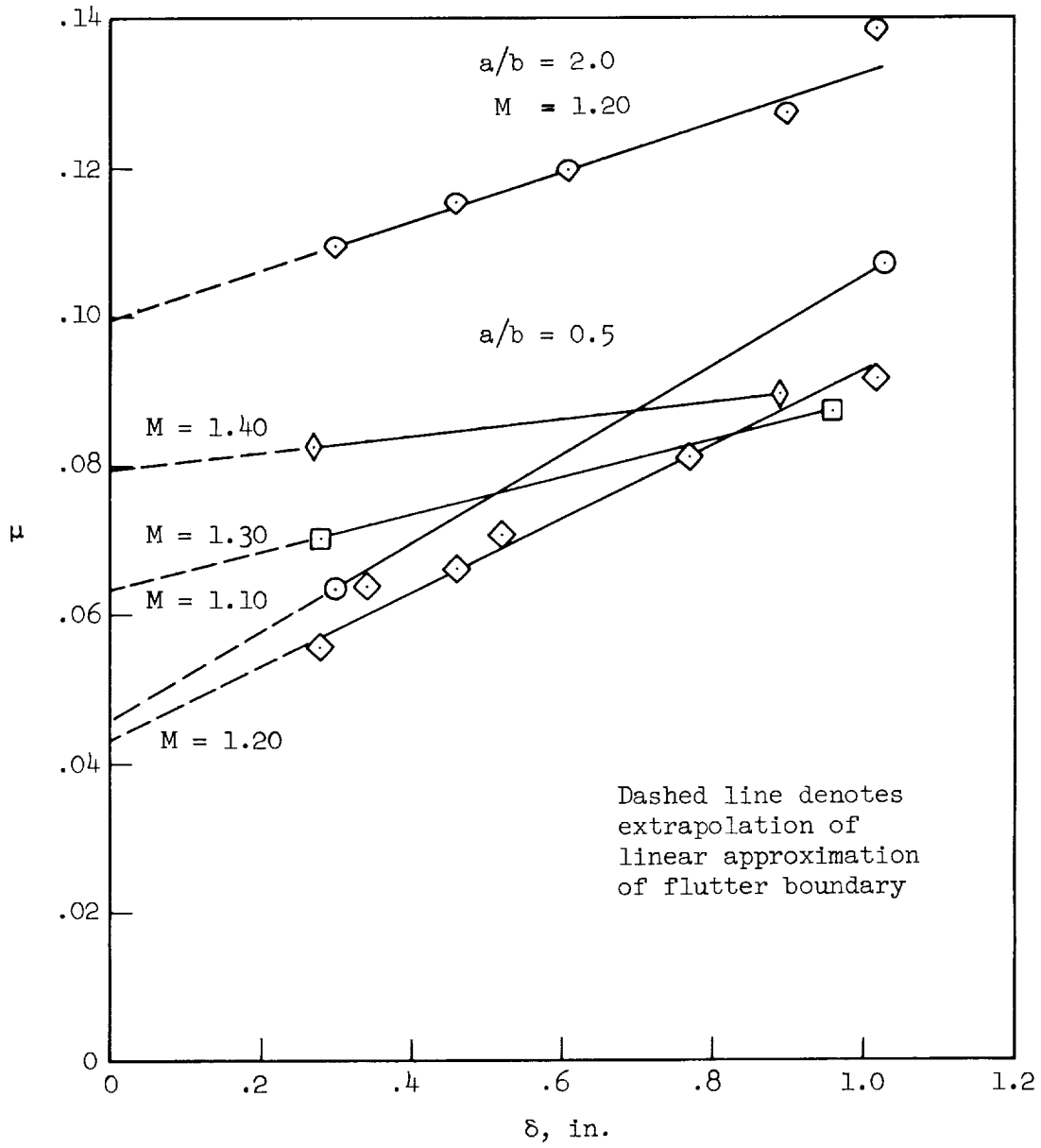


Figure 31.- Mass ratio parameter as a function of boundary-layer thickness.

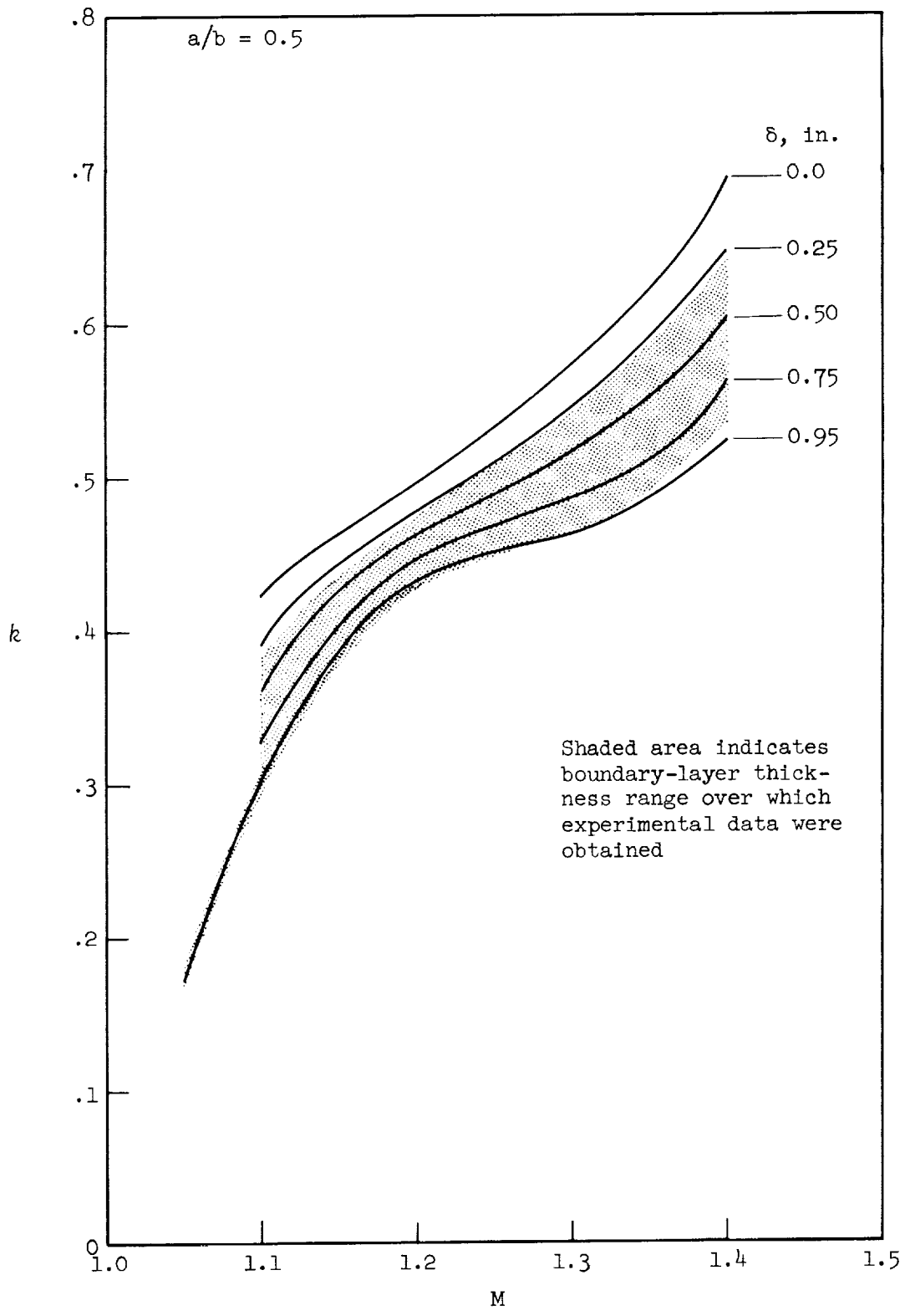


Figure 32.- Reduced frequency of flutter as a function of Mach number.

